LITHIUM RECOVERY FROM WATER BY GRANULATED PVC/PAN-TITANIUM TYPE LITHIUM ION-SIEVE

A Thesis Submitted to
the Graduate School of Engineering and Sciences of
İzmir Institute of Technology
in Partial Fulfillment of the Requirements for the Degree of

MASTER OF SCIENCE

in Chemical Engineering

by
Onur İPEK

July 2024
İZMİR

We approve the thesis of **Onur İPEK**

Examining Committee Members:

Prof. Dr. Aslı YÜKSEL ÖZŞEN
Department of Chemical Engineering, İzmir Institute of Technology

Doç. Dr. Ayben TOP
Department of Chemical Engineering, İzmir Institute of Technology

Doç. Dr. Canan URAZ
Department of Chemical Engineering, Ege University

10 July 2024

Prof. Dr. Aslı YÜKSEL ÖZŞEN
Supervisor, Department of Chemical Engineering
İzmir Institute of Technology

Prof. Dr. Aysun SOFUOĞLU
Head of the Department of
Chemical Engineering

Prof. Dr. Mehtap EANES
Dean of the Graduate School of
Engineering and Sciences

ACKNOWLEDGEMENTS

I would like to express my deepest gratitude to my advisor, Prof. Dr. Aslı Yüksel Özşen, for her unwavering belief in me and providing me with this invaluable opportunity. Working under your mentorship has been an enlightening and enriching experience for which I am profoundly grateful.

I am truly grateful for the endless support and guidance provided by the Yaşar Kemal Recepoğlu, Bahriyenur Arabacı, and Bulutcem Öcal. Your collaboration and constructive feedback have been essential to my research journey. I have been privileged to work alongside such talented and dedicated individuals.

I owe my deepest gratitude to my family, Zerrin İpek, Ömür İpek, Halil İpek, Göksun İpek, Alya İpek, and Mira İpek. Your unwavering love and constant encouragement made this and all other achievements possible. I share this success with you, for it belongs to you as much as it does to me. Your belief in me has made everything possible, and I am forever grateful for your presence in my life.

I would also like to express my heartfelt gratitude to my dear friends Görkem Taylan, Gökberk Aktuna, and Büşra Sezen. You have been my steadfast pillars of strength and sources of joy. In moments when life's challenges seemed overwhelming, you were always there to support and uplift me. Your unwavering friendship and companionship have been invaluable. I am deeply grateful to have such incredible three friends who have enriched my life in countless ways.

Last but certainly not least, I want to extend my most heartfelt thanks to my beloved partner, Özüm Özbek. Your unwavering belief in me has been my driving force throughout this journey called life. Your encouragement during the toughest times and your constant reassurance have kept me going when I felt like giving up. You celebrated my smallest victories and stood by me through my biggest challenges, reminding me of my strengths and potential. Your love and understanding have been a source of immense comfort and motivation. Even in my darkest days, you were my guiding light, lifting me up when I lost my motivation and hope. Thank you for being my greatest support, my source of endless inspiration, and the love of my life.

ABSTRACT

LITHIUM RECOVERY FROM WATER BY GRANULATED PVC/PAN-TITANIUM TYPE LITHIUM ION-SIEVE

Lithium consumption and the need for production have been in rising trend due to increase in electric vehicles and energy storage systems. Lithium was nominated as a critical element, which means that it has no substitute. Also, the majority of the lithium was dissolved in brines, untouched. Therefore, this study investigated the performance of titanium-based lithium ion-sieve which was synthesized by solid-phase change method and immobilized by granulation with PVC and PAN polymers for lithium recovery from water bodies. The granulated adsorbent, PVC/PAN-HTO, was characterized by FT-IR, BET, XRD, and SEM analyses which revealed that material successfully synthesized. Moreover, batch adsorption experiments were carried out to investigate performance. Lithium recovery occurs in alkaline medium as the point of zero charge being 6.03; below this pH level, lithium stripping takes place. Optimum lithium recovery rate of 98.7% was achieved at pH 12 using a 4 g/L adsorbent dosage in model lithium solution, while in geothermal water, with the same adsorbent dosage, a recovery rate of 91.6% was attained. Kinetic study revealed the rate constants of the reaction for pseudo first and second order, while the latter fits better. Langmuir isotherm at 25 °C, which resulted maximum adsorption capacity of 5.59 mg/g, showed better fit for explanation of the adsorption behavior. Thermodynamic calculations showed that the adsorption was endothermic and spontaneous. Cycling tests showed that there was no significant decrease in lithium recovery rate after three adsorption-desorption cycles. Results indicate that the granulated adsorbent, PVC/PAN-HTO, was lithium selective, promising, and reusable.

ÖZET

GRANÜLE EDİLMİŞ PVC/PAN-TİTANYUM TİPİ LİTYUM İYON ELEK İLE SUDAN LİTYUM GERİ KAZANIMI

Elektrikli araçların ve enerji depolama sistemlerinin artması nedeniyle lityum tüketimi ve üretim ihtiyacı artış trendindedir. Muadili olmamasından dolayı kritik element olarak sayılan lityumun büyük kısmı su kaynakları içinde çözünmüş haldedir. Bu nedenle bu çalışma katı faz değişimi yöntemi ile sentezlenmiş toz halindeki titanyum bazlı lityum iyon eleği (HTO) immobilize etmek için PVC ve PAN polimerleri ile granüle edilmiştir ve su kütlelerinden lityum geri kazanımı için test edilmiştir. Elde edilen adsorbent, PVC/PAN-HTO, FT-IR, BET, XRD ve SEM analizlerini kullanarak karakterize edilmiştir ve performansı batch adsorpsiyon çalışmalarıyla test edilmiştir. Adsorbentin lityumu tutabilmesi için ortamın bazik olması gerektiği görülmüş ve malzeme için sıfır yük noktası olarak pH 6.03 değeri bulunmuştur. Model lityum çözeltisinde 4 g/L adsorban dozajı kullanılarak pH 12'de %98.7'lik optimum lityum geri kazanım oranı elde edilirken, jeotermal suda aynı adsorban dozajı ile %91.6'lık bir geri kazanım oranı elde edildi. Psödo-birinci ve ikinci derece reaksiyon sabitleri kinetik çalışmalar tarafından ortaya konuldu. 25 °C'deki Langmuir izotermi adsorpsiyon davranışını daha iyi açıklarken maksimum adsorpsiyon kapasitesini 5.59 mg/g olarak sonuçlandırdı. Termodinamik hesaplamalar adsorpsiyonun endotermik ve kendiliğinden olduğunu gösterdi. Üç adsorpsiyon-desorpsiyon döngüsünden sonra lityum geri kazanım oranında önemli bir azalma olmadığı görüldü. Sonuçlar, granül adsorban PVC/PAN-HTO'nun lityum seçici, umut verici ve yeniden kullanılabilir olduğunu göstermektedir.

TABLE OF CONTENTS

LIST OF FIGURES

Figure **Page**

Figure **Page**

LIST OF TABLES

Table **Page**

LIST OF ABBREVIATIONS

Abbreviation	Definition
$\Delta G°$	Gibbs free energy change
$\Delta H°$	Standard enthalpy change
$\Delta S°$	Standard entropy change
AABs	Alpha-alumina beads
AD	Adsorbent dosage
BET	Brunauer-Emmett-Teller
BJH	Barrett-Joyner-Halenda
CA	Cellulose aerogels
CAM	Cellulose acetate membrane
CTS	Chitosan
DMAc	N,N-dimethylacetamide
DMF	N,N-dimethylformamide
ECH	Epichlorohydrin
EDGE	Ethylene glycol diglycidyl ether
EVAL	Poly(ethylene-co-vinyl alcohol)
FT-IR	Fourier-transform infrared spectroscopy
GA	Glutaraldehyde
HMO	Hydrogen manganese oxide
HTO	Hydrogen titanium oxide
ICP-OES	Inductively coupled plasma optical emission spectroscopy
K_L	Langmuir isotherm constant
LIS	Lithium ion-sieve
LMO	Lithium manganese oxide
LTO	Lithium titanium oxide
PAM	Polyacrylamide
PAN	Polyacrylonitrile
PEG	Polyethylene glycol
PSF	Polysulfone
PVA	Polyvinyl alcohol
PVC	Polyvinyl chloride
PVDA	Polyvinylidene fluoride
PVDF	Polyvinylidene difluoride
PZC	Point of zero charge
q_e	Adsorption capacity at equilibrium
q_{max}	Maximum adsorption capacity
RPM	Revolutions per minute
SEM	Scanning electron microscope
XRD	X-Ray diffraction analysis

CHAPTER 1

INTRODUCTION

Preventing greenhouse gas emissions became a phenomenon as it serves to climate change which is one of the most important issues in today's world. Also, elimination of the use of fossil fuels is crucial. Therefore, many environmental actions and regulations have been implemented. For example, many incentives are taken to implement renewable energy such as wind turbines, solar energy, and hydrothermal energy. Also, the use of electric vehicles have gained popularity. However, in order to store the energy, energy storage systems, so called lithium-ion batteries are required. As the name implies, these systems require lithium metal and there are no substitute. Consequently, global lithium consumption in 2023 was 180,000 tons which was 27% higher than the previous year. This increase is 600% compared to the last decade.[1,2]

Until 1980, lithium extraction relied exclusively on ores; today, the majority of lithium is still obtained from mineral ores.[3,4] In the world, approximately 105 million tons of lithium resources exist while only the 40% of it exist as the lithium mineral ores.[2,5,6] Moreover, lithium reserves are unevenly distributed and its usage rate significantly increasing. Therefore, there is high interest in the alternative lithium recovery from the remaining 60% of the lithium reserves which are buried under the water resources such as continental brines, geothermal brines, and oilfield brines.[5]

To be able to recover lithium from the water sources, over the years, many lithium recovery methods are suggested which are solar evaporation, evaporative crystallization, solvent extraction, co-precipitation, electrochemical techniques, adsorption and so forth. Among all, adsorption techniques stands out as a promising method as it is eco-friendly, efficient, simple, and green process. Disadvantage of the adsorption method is not having an appropriate adsorbent for industrial applications.[3] This study aims to fill this gap.

For the lithium recovery from the brine waters, a material called lithium ion-sieves (LIS) are used. These materials has good lithium screening performance as they have stable molecular framework. Thus, lithium recovery from the brines are possible at high rate and high selectivity. Nevertheless, these materials can be produced in powdery form which is not practical to be implemented in the industrial processes as they result poor liquidity, insufficient permeability, difficulty in handling, post-separation problems, and

high energy consumptions due to the higher pressure drops.[7] Also, since the adsorption and desorption processes occur under strong alkali and acidic conditions, stability of the immobilized material is important. Therefore, researchers studied the immobilization of the powder LISs, and different methods are suggested such as foaming, fiber formation, magnetization, membrane formation, and granulation.[6] Among all, granulation is a promising technique in nanoparticle modification, offering granulated LISs with high water permeability, mechanical and chemical stability.[6,8]

For granulation, polymer matrix usage is one of the most effective approaches for the granulation method. Accordingly, different polymers are suggested such as chitosan, agar, cellulose, alpha-alumina beads (AABs), polyacrylamide (PAM), polyvinyl alcohol (PVA), polyacrylonitrile (PAN), and polyvinylchloride (PVC).

The scope of this study includes the search for an adsorbent which is applicable to use in industrial process for lithium recovery from brine waters. For this matter synthesis of titanium type lithium-ion sieve granulated with the combination of PVC and PAN polymer. Titanium type adsorbents have the advantages of being better in stability and therefore environmentally friendly. On the other hand, PVC is a hydrophobic material which is good for the stability of the adsorbent while hydrophobic property hinders the adsorption capacity as it rejects the water to flow through adsorbent channels. Therefore, combination of PVC with hydrophilic polymer, namely PAN, are suggested.

Synthesized material characterized via FT-IR, BET, SEM, and XRD. The proposed material was tested with model lithium solution and its performance was also tested with geothermal water for certain experiments. Through the study, batch experiments were used to investigate the key adsorption factors of lithium recovery such as pH, adsorbent dosage, adsorption kinetics, isotherms, desorption, cycling, and thermodynamics.

CHAPTER 2

LITERATURE SURVEY

2.1. Significance of Lithium

Lithium element has the atomic number of 3 which makes it the smallest and the least dense metal. Due to being the lightest metal, lithium has many applications such as pharmaceuticals, ceramics and glass, lubricant greases, air conditioning, dyes, continuous casting, polymer composites, aerospace parts, and the most importantly batteries.[2,9] Global lithium consumption in 2023 was 180,000 tons which was 27% higher than the previous year, while it was 600% higher than the last decade.[1,2] To mitigate greenhouse gas emissions, environmental actions and regulations have been implemented such as use of electric vehicles and integration of renewable energy which uses energy storage systems. Also, due to the growth in population and urbanization, the number of portable electronic devices have been increasing. Consequently, lithium-ion batteries have become the major contributor to the lithium consumption with approximately 87%.[2] Also, demand on lithium expected to be increasing exponentially.[10] Thus, lithium is considered a critical element since the reserves were geographically concentrated and notably being limited.[11] Expected rise in lithium use in four different scenarios were represented in Figure 2.1.

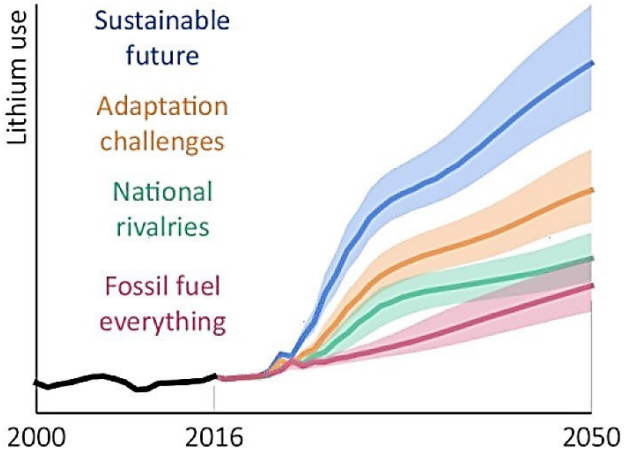

Figure 2.1. Estimation of lithium usage in four different scenarios[12]

2.2. Lithium Sources

Lithium resources were categorized in two: the lithium mineral ores, which encompass pegmatite, spodumene, hectorite, and other variants; and lithium water resources, including continental brines, geothermal brines, and oilfield brines. According to Swain et al., distribution of lithium reserves was given in Figure 2.2.[5] Until 1980, all the lithium extracted was solely from ores; at present, the majority of the extracted lithium still comes from the mineral ores.[3,4] Moreover, approximately 105 million tons of lithium resources exist and more than 60% of the global lithium amount is in the water resources.[2,5,6] Due to the uneven global distribution of lithium and the increasing demand alongside the potential shortage, there has been a notable surge in interest towards lithium recovery from brines.[13,14]

Figure 2.2. Lithium distribution in terms of source (derived from Swain et al.[5])

2.3. Lithium Recovery Methods

Various methods have been suggested over the years for the recovery of lithium from brine waters including solar evaporation, chemical precipitation, solvent extraction, membrane, electrochemical techniques, bioaccumulation, adsorption and so forth. In this section explanations of the methodologies, advantages and disadvantages of these methods have been addressed. General advantages and disadvantages of lithium recovery methods were given in Table 2.1.

Table 2.1. Comparison of lithium recovery methods

Method	**Advantages**	**Disadvantages**
Solar Evaporation	Simple Readily available	Time consuming High cost Requires vast land area Low purity of product
Precipitation	Mature process Highly reliable Low cost	pH sensitive Only appropriate for low-grade brines
Solvent Extraction	High purity of product Simple process	High corrosivity Low recovery Pollution
Membrane Technology	Energy efficient Low environmental impact	Poor durability
Adsorption	Simple process Efficient Eco-friendly Economical	Lack of adsorbent for industrial operations

Solar evaporation covers the evaporation of water by solar energy followed by elimination of impurities by precipitation. Method is conventional but industry standard for recovery of lithium. Lithium ions in brines, as well as other minerals and metal salts, were concentrated by evaporation of water. Then unwanted metal salts were precipitated chemically. Even though it is an easy method, requires vast land areas and natural evaporation of water time consuming. Also, other cations inhibit the production of high purity lithium.[3] Brines of Northwest of Argentina were investigated in a study and after precipitations of NaCl, KCl, $CaSO_4$, and $Mg(OH)_2$ by use of chemical reagents, concentration of lithium ion was increased from 900 to 7200 ppm when 64.3% of

evaporation volume reached.[15] This study stated that the lithium recovery was 28.1% at a brine yield of 33.5% and the purity of the recovered.

In the precipitation method, a chemical precipitant is added to lithium-containing brine to cause lithium ions to react and form a solid precipitate, which is then separated and processed to obtain pure lithium compounds. Among the chemical precipitants tested aluminum-based salts such as $AlCl_3$ were shown the best performance for lithium recovery.[16] However, Alsabbagh et al. were performed chemical precipitation method on evaporated brine water of Dead Sea applied and concluded that tri-sodium phosphate was a promising reagent.[17] The results of the study showed that lithium concentration can be enriched 50 times more compared to initial concentration. Despite being a highly reliable process with low cost, method is sensitive to temperature and pH for promising result and only applicable for low-grade brine resources.[3]

Solvent extraction recovers lithium by dissolving the lithium in brine with an organic solvent and then separating it from the solvent. This method is simple to use for industrial applications with the possibility of high purity Li^+ recovery.[18] Zhou et al studied lithium recovery from salt-lake brines by using solvent extraction with tributyl phosphate as extractant and $FeCl_3$ as co-extraction agent.[19] Under the optimum conditions the authors experimented with, extraction efficiency of lithium ion reached up to 65.53% with the strong Li^+ selectivity, compared to Mg^{2+}, K^+, and Na^+. However, as the name implies, the method includes solvent usage which results in chemical and environmental risks. Also, method suffers from low recovery rates with the possibility of corrosion of the equipment.[3]

Since lithium is the smallest among all metals, membrane technology is suitable for the recovery of lithium forum brines. Therefore, reverse osmosis and electrodialysis were suggested. Reverse osmosis acts as water removal and thus lithium concentration. However, it is said that reverse osmosis is not economically feasible to use on brines as brines have high concentrations and include complex salts.[20] On the other hand, electrochemical separation, namely dialysis, is a process that employes electrical field to facilitate ion movement through a membrane. Ni et al. examined the monovalent selective ion-exchange membranes on model Li^+/Mg^{2+} solution and concluded that the 95.3% lithium recovery with high selectivity.[21] Despite its potential, being energy efficient, and low environmental impact, ionic membranes suffer from poor durability which limits its industrial application.[20]

Adsorption is the process by which molecules of a gas or liquid that come into contact with a surface or substance are retained by the surface. This phenomenon occurs due to intermolecular forces of attraction and usually occurs on a solid surface. Adsorption is widely used in various industrial and scientific applications, especially playing an important role in cleaning gases, catalysis, and separation processes. Adsorption technique involves the use of adsorbent materials to selectively capture lithium ions from brine solutions via physisorption or chemisorption. Adsorption appears as a promising technique among others as it is eco-friendly, economical, efficient, simple, and green process. However, in adsorption, significant challenge arises since method has the drawback of absence of adsorbents for industrial applications.[3]

2.4. Lithium Ion-Sieves

Ion-sieve oxides are the type of adsorbents that have the ability to selectively screen the metal-ions. Tailoring of the ion-sieves are possible by forming them by the precursor of the target metal-ion, such as $LiCO_3$ or LiOH in the case of lithium recovery. Hence the derived sorbent named as Lithium Ion-Sieve (LIS). LISs have a stable molecular structure, hence even when the target ions are stripped from the crystal sites, these sites remain intact and available for further adsorptions. The vacant sites were created by lithium thus the size of the vacant sites was also tailored. Therefore, only atomic radii of equal or lower than the target metal-ion can be absorbed on these sites. Since lithium has the smallest atomic radius compared to all metals, high selectivity for lithium adsorption can be achieved via LISs.[6] In Figure 2.3, the working principle of LIS as aforementioned procedure were given. As from production, ion-sieves are filled with Li^+ ions that come from precursor. In order to activate the ability of lithium adsorption, these ions should exchange with H^+ ions. This step was also nominated as delithiation. Once the LIS is in hydrogen filled state, the adsorbent is ready for adsorption of lithium from lithium containing solution. While adsorption, H^+ ions that are present in the framework exchange with Li^+ ions and form the LIS in lithium filled state. By the regeneration (desorption) of the LIS, the material turns back to its hydrogen filled state and ready to further adsorption process. The recovered lithium will then be present in the

regeneration eluent. After the delithiation, each adsorption/desorption loop counts as a cycle, and the number of achievable cycles determines the stability of the LIS.

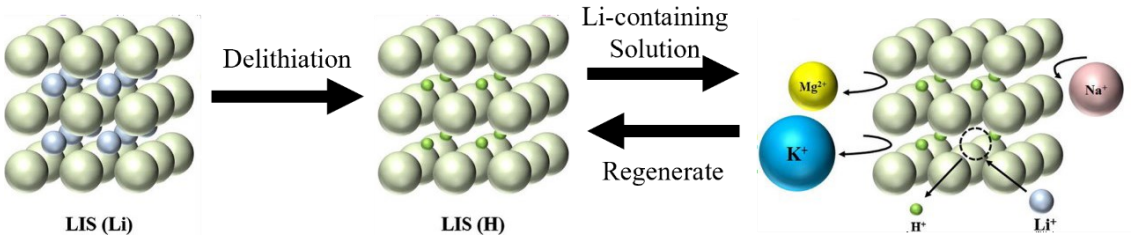

Figure 2.3. Working principle and life cycle of LISs (derived from Xu et al.[6])

LISs were classified into two main categories: manganese-based LIS (Mn-LIS, HMO, or LMO) and titanium-based LIS (Ti-LIS, HTO, or LTO). Mn-LISs are the most used adsorbent for this duty as it results in high lithium adsorption capacity and selectivity.[14] However, Mn-LISs suffer from Mn-loss during operation leading to the poor cycling performance of the material.[3,22] On contrary, due to the stronger Ti-O bond than Mn-O bond, Ti-LISs have more stable structure than Mn-LIS, resulting less dissolution loss and better cycling performance.[23,24] Moreover, even if titanium species dissolute to the water body, unlike manganese, it can be readily removed from aqueous solution and titanium poses no threat to aquatic environment.[6]

Li et al. studied the different phases of TiO_2 (amorphous, rutile, and anatase) as the reactant of the LTO.[25] Three variations of LTO were synthesized by the solid-state reaction method. Findings were concluded that the performance is in correlation with the wettability, hydrophilicity, of the adsorbent. Contact angle, which is a method for measuring hydrophilicity, were measured, and determined as 49°, 38°, and 14° for rutile, amorphous, and anatase crystalline phases of TiO_2, respectively. Hence, anatase is the most hydrophilic state among the phases which means it yields easy transfer for H^+ and Li^+. Increase in hydrophobicity changed the adsorption capacity from 9.83 to 18.33 and 34.48 mg/g for rutile, amorphous, and anatase phases, respectively.

Chitrakar et al. performed the synthesis of H_2TiO_3 by solid-phase calcination method and at the pH of 6.5, achieved 32.6 mg/g Li^+ adsorption capacity.[23] Also, high

selectivity toward Li^+ were observed with the selectivity order of following: $Li^+ >> Na^+ > K^+ > Mg^{2+} > Ca^{2+}$, due to the size effect of the ions.

Moazeni et al. performed hydrothermal synthesis of $Li_4Ti_5O_{12}$ lithium adsorption capacity of 39.43 mg/g.[26] The synthesized material showed nanotube morphology with 50-70 nm in diameter and 1-2 micrometer in length.

A spinal type $Li_4Mn_5O_{12}$ was synthesized via solid-phase reaction by Xiao et al. which resulted in lithium adsorption capacity of 39.62 mg/g at pH of 10.1 by use of model lithium solution derived from LiCl. Except Mg^{2+}, almost full rejection was observed for other competitor ions. 55 cycles of adsorption-desorption experiment were carried out and the adsorption capacity were kept at 2.78 mg/g.[27]

Xiao et al. conducted the synthesis of spinel $Li_{1.}6Mn_{1.6}O_4$ which resulted in a high lithium adsorption capacity of 42.1 mg/g at the pH of 10.01. After six adsorption desorption-cycles adsorption capacity were decreased from 28.36 mg/g to 25.15 mg/g by 11.33% decrease, while having high selectivity toward lithium.[28]

$LiMn_2O_4$ were synthesized by Zhang et al and at the pH of 9.19 adsorbent yield Li^+ adsorption capacity of 16.9 mg/g. The selectivity order was high for Li^+, followed by divalent ions Ca^{2+} and Mg^{2+} then K^+ and Na^+ which are monovalent ions.[29]

2.5. Immobilization of Lithium Ion-Sieves

LISs comes in powdery form once synthesized, hence it is difficult and impractical to use these adsorbents in industrial column operations. In column adsorption, use of powder material resulting in poor liquidity, insufficient permeability, difficulty in handling, post-separation problems, and high energy consumptions due to the higher pressure drops.[7] To immobilize the powder LISs methods such as foaming, fiber formation, membrane formation, and granulation have been suggested. These methods form adsorbents that allow to use in industrial column operations. However, compared to LIS powder, such methods inhibit adsorption capacity (q_e) and kinetic properties. Thus, the researchers aim to synthesize an adsorbent with performance equal or close to powder LIS. The Table 2.2 at the end of this chapter outlines the studies that will be mentioned for immobilization of LISs and more.

2.5.1. Foam Forming

Nisola et al. performed the foam forming on LIS ($H_{1.6}Mn_{1.6}O_4$) by polyvinyl alcohol (PVA) and yielded insoluble and flexible adsorbent.[30] Images of the synthesized material were given in the Figure 2.4. Varying loading rates were tested and 250 wt% LIS/PVA were found to be best in the range of experiment due to having the most adsorption capacity and durability. Suggested adsorbent resulted in combined microporous and mesoporous by cryo-desiccation. The approximate performance of LIS was achieved, due to the high surface area and hydrophilicity of used polymer (PVA), and high LIS loading. Adsorption performances were tested on model lithium solution and retained 91% adsorption capacity of the LIS used in the study.

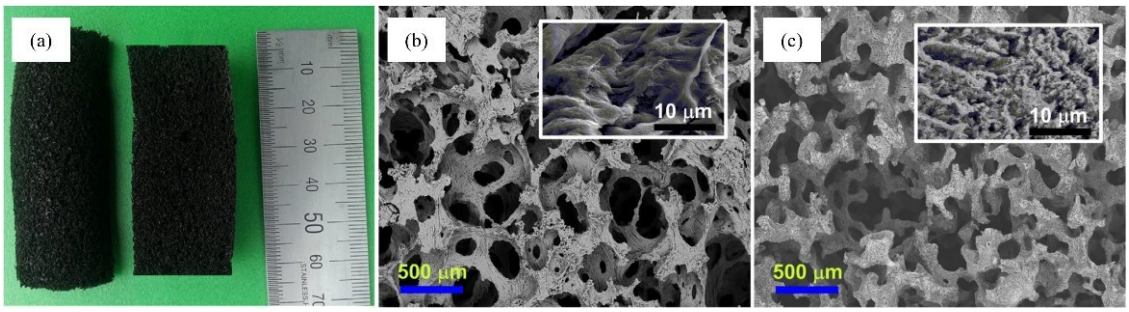

Figure 2.4. Images of selected PVA/HMO (a) optical image of the foam adsorbent (b) SEM image of PVA foam (c) SEM image of the 250 wt% LIS/PVA[30]

Ma et al. studied foam forming by polyurethane template method on spinel manganese oxide and obtained composite had combination of meso- and macroporous structure.[31] The adsorption experiment was conducted on model lithium solutions of LiOH and LiCl, and Salt Lake brine which resulted Li^+ adsorption capacities of 8.73, 3.82, and 1.46 mg/g, respectively. Owing to ion-sieve effect, selectivity toward Li^+ ions were seen, and selectivity sorted as follows: $Li^+ >> Mg^{2+} > K^+ > Na^+$.

Limjuco et al. used the H_2TiO_3 LIS and PVA to obtain foam type composite.[32] Compared to LIS, composite retained 94% Li^+ at the optimum determined LIS loading of

200 wt%. Consecutive adsorption-desorption performance of the composite adsorbent showed that its mechanical and chemical strength remained for 5 cycles.

2.5.2. Fiber Formation

Unique structure of nanofibers with high specific area and porosity and unique mechanical strength, fiber formation also had increased attention.[33] Fiber adsorbent was synthesized by the help of electrospinning method of the mixture of polymer and LIS in a solvent.

By Park et al., Polyacrylonitrile (PAN) were used with HMO ($H_{1.6}Mn_{1.6}O_4$) LIS.[34] Electrospinning method was utilized with varying HMO loadings on PAN, and composite fiber diameter less than 300 nm were formed. At the loading of 60 wt% HMO to PAN, the highest adsorption capacity of Li^+ of 10.3 mg/g was seen which was 96% of HMO. Also, after ten adsorption-desorption cycles the adsorption performance remained similar. The ion-sieve effect resulted selective Li^+ adsorption and Ca^{2+} was the most competitor ion with the α_{Ca}^{Li} value of 224.

Polysulfone (PSF) and HTO (H_2TiO_3) were mixed in N-methyl pyrrolidone to form porous fiber adsorbent by electrospinning method in the study of Zhao et al.[35] In Figure 2.5, optic and SEM images of the synthesized nanofiber were given. At the HTO loading of 50 wt% to PSF usage, similar adsorption performance was seen compared to powder HTO. Equilibrium adsorption capacity for lithium were determined as 30.51 mg/g for model lithium solution and 22.66 mg/g for geothermal water with the contact time of one hour. The separation factor α_{Me}^{Li} were calculated higher than 872 for all competitor ions.

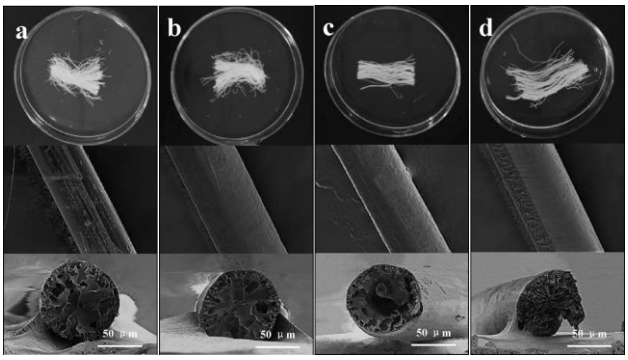

Figure 2.5. Optic and SEM images of fiber adsorbents of different polymers (a) Polystyrene (b) Polyacrylonitrile (c) Polyvinyl chloride (d) Polysulfone[35]

Lawagon et al. performed different polymers of PVC, PVDF, PSF, and PAN with HTO (H_2TiO_3) to form nanofibers via electrospun method.[36] Among all, due to its hydrophilicity, PAN polymer resulted in the best outcome. Maximum adsorption capacity of 72.75 mg/g was determined by Langmuir adsorption isotherm, on model lithium solution, which is significant. No difference in adsorption capacity was observed after five adsorption-desorption cycles.

2.5.3. Membrane Formation

Membrane formation is one of the promising methods for immobilization of LISs. Compared to granulation, which will be discussed later in, membrane adsorbents have the advantage of ease in construction by stacking or winding the membranes and allowing them to suitability for industrial continuous operation.[14] In contrast, membrane forming is economically infeasible and complicated.

In the study of Umena et al., spinel manganese oxide ($Li_{1.33}Mn_{1.67}O_4$) and poly vinyl chloride (PVC) were employed via solvent exchange method, using N,N-dimethylformamide (DMF) as solvent.[37] As the lithium containing solution, seawater at stable velocity of 1.25 cm/min. Study revealed that the adsorption capacity is highly relied on preparation conditions. Adsorption of the membrane followed Freundlich model and Li^+ uptake value determined to be 16 mg/g while HMO itself resulted 22 mg/g.

Method of membrane forming were performed by Zhu et al. by using solvent exchange method.[38] As solvent N,N-dimethylacetamide (DMAc) were used while PVC and $Li_{1.6}Mn_{1.6}O_4$ were used as binder and precursor, respectively. Varying PVC ratios were tested, and it was found that at and below the concentration of 6 wt% a very soft membrane was formed which is not suitable for adsorption. Also, increase in PVC concentration resulted in a decrease in adsorption capacity approximately from 9.25 to 7.6 mg/m^2, when PVC loading increased from 8 to 16 wt%, respectively. Moreover, at 10 wt% PVC loading, varying concentrations of LMO were tested. Adsorptive capacity was increased approximately from 4.2 to 10.5, while LMO loading increased from 5 to 25 wt%, respectively. Cycling performance was also evaluated for the membrane with 10 wt% PVC and 15 wt% HMO. It was found that after 8 cycles, adsorption capacity decreased by only 2%. Rather than Freundlich, Langmuir adsorption model strongly fits the adsorption of the suggested membrane and at 298 K adsorption capacity of 11.49 mg/m^2 calculated. Study also proved that the resulting membrane is highly dependent on preparation conditions and membrane thickness.

Sun et al. performed phase inversion method of mixed casting solution with Polyvinylidene fluoride (PVDA) as binder, HMO ($H_4Mn_5O_{12}$) as precursor, and DMAc as solvent.[39] Model lithium solution of 100 ppm was used for the effective membrane area of 4.8 cm^2. Maximum adsorption capacity was calculated as 27.8 mg/g with the contact time of one hour. Also, suggested membrane's Li^+ selectivity resulted the separation factor (α_{Mg}^{Li}) was 4.76, compared to Mg^{2+}. The adsorption performance remained for six adsorption-desorption cycles.

2.5.4. Granulation

Granulation is the most commonly used and known nanoparticle forming method.[14] Adsorption and desorption processes of lithium ion by LISs occur under strong alkali and acidic conditions, respectively. Therefore, among the other methods, granulation is the promising technique in nanoparticle modification, offering granulated LISs with high water permeability, mechanical and chemical stability.[6,8] Method includes the use of polymers as binders. In the literature, various materials were suggested for this

purpose, including organic polymers such as chitosan, agar, and cellulose; as well as inorganic polymers like alpha-alumina beads (AABs), polyacrylamide (PAM), polyvinyl alcohol (PVA), polyacrylonitrile (PAN), and polyvinyl chloride (PVC) have been suggested.

Selection of polymer for the granulation procedure is crucial in determining the performance of the adsorbent. The hydrophobicity/hydrophilicity and the morphology of the chosen binder are fundamentally important for achieving high-performance adsorbent. Morphology of the material surely determines the granulated adsorbent pore volume, pore size, and surface area. However, hydrophobicity/hydrophilicity of the material holds greater importance. In Figure 2.6, quantified hydrophobicity of the common polymers was given according to molecular level method.[40] As the rule of thumb, hydrophobic binders result in high mechanical and chemical strength and longer adsorption-desorption cycles, while decreasing maximum adsorption capacity that LIS has, by inhibiting the diffusion ability of target metal ion. On the other hand, hydrophilic binders result in closer adsorption capacity to powdery LIS has, however decreases the stability of the adsorbent as it allows the water flow through the adsorbent.

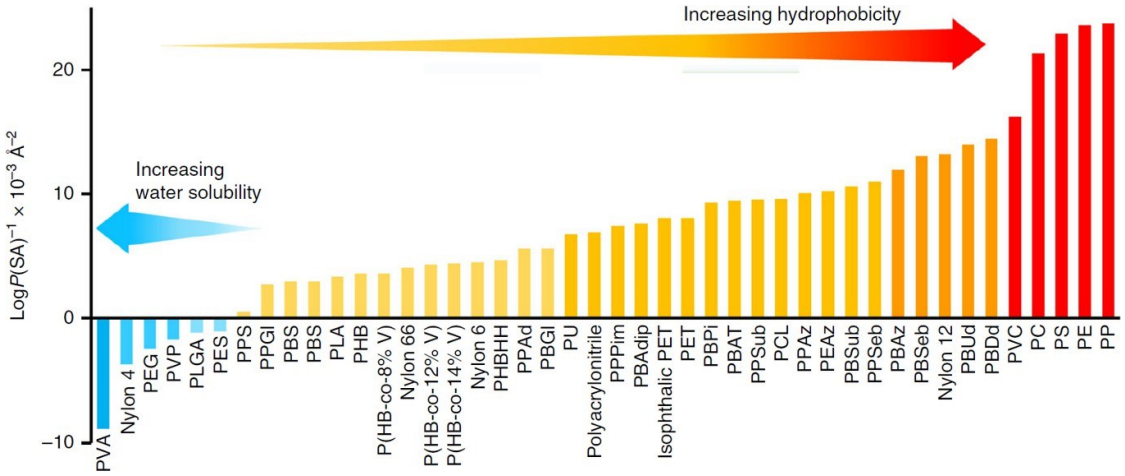

Figure 2.6. Hydrophobicity of various plastics[40]

Because of the biodegradability and hydrophilicity Wang et al. performed granulation of LMOs ($LiMn_2O_4$, $Li_4Mn_5O_{12}$ and $Li_{1.66}Mn_{1.66}O_4$) by Chitosan (CTS).[41] However, as the CTS contains hydroxyl and amino groups, it is prone to dissolution loss

under acidic conditions. Thus, authors also experimented with various crosslinking reagents of glutaraldehyde (GA), epichlorohydrin (ECH), ethylene glycol diglycidyl ether (EDGE) to bind CTS to LMO. In the Figure 2.7, granulation and crosslinking procedure were given. As the powdery LMO, it is found that $Li_4Mn_5O_{12}$ had the highest adsorption performance among all this granulation were performed on this adsorbent while the crosslinking agent of EDGE resulted the lowest dissolution loss. The suggested optimum combination, CTS/$Li_4Mn_5O_{12}$ crosslinked with EDGE, was tested on geothermal water sampled from wellbore located in Tibet. The adsorbent was followed the Langmuir isotherm model and found that the maximum adsorption capacity (q_{max}) of 11.58 mg/g while the equilibrium capacity resulted the 8.98 mg/g adsorption capacity at 303 K within the contact time of 24 hours. Furthermore, adsorption capacity decreased 1.1% after five cycles.

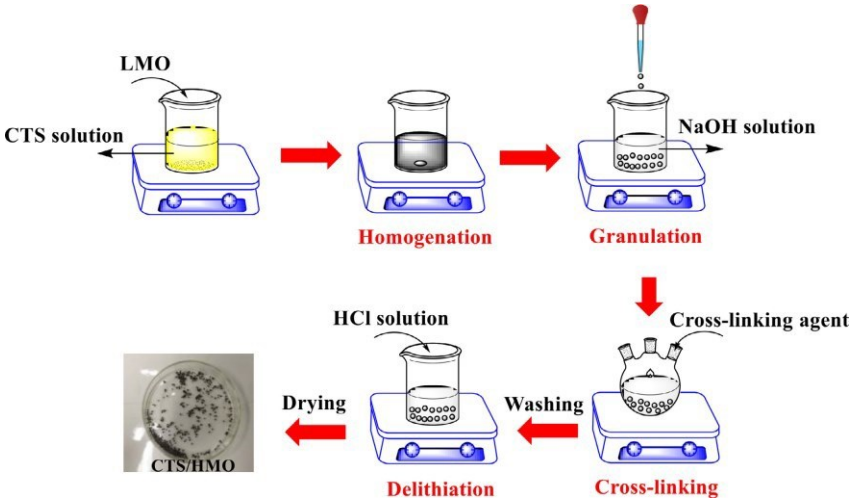

Figure 2.7. Preparation procedure of cross-linked CTS/HMO[41]

Qian et al. performed granulation of H_2TiO_3 with Cellulose Aerogels (CA) by freeze drying method which is a green matrix as it is a biomass polymer.[42] The proposed adsorbent demonstrated the Li^+ adsorption capacity of 28.61 mg/g at 35 °C, in accordance with the Langmuir adsorption isotherm. Experiments were also carried out by using sea water obtained from Bohai Sea near Yingkou. Adsorption capacity of lithium in geothermal water resulted in 25.8 mg/g, whereas the competitor ions Mg^{2+}, Ca^{2+}, Na^+,

and K^+ were exhibited 4.45, 3.72, 0.44, 0.94 mg/g adsorption ,respectively, after 24 hours of contact time at room temperature.

Xiao et al., by using the anti-solvent method, synthesized 2.0 to 3.5 mm spherical ion sieve by using PVC and $Li_4Mn_5O_{12}$ in N-methyl-2-pyrrolidone as solvent.[43] The study conducted both batch and continuous adsorption and desorption configurations. 23.47 mg/g of maximum Li^+ adsorption capacity at the temperature of 324.4 K were determined and decreased to 19.84 mg/g at 304.5 K, according to highly correlated Langmuir adsorption isotherms. In the column adsorption, model solutions were utilized with 6 different ion concentrations to simulate the brines from salt lakes. In the presence of Mg^{2+}, Na^+, and K^+, adsorbent showed good selectivity towards Li^+ by enriching the concentration of Li^+ in the feed solution up to 17 times. The study group later granulated the $Li_4Mn_5O_{12}$ by Polyacrylamide (PAM) and obtained 0.3-0.7 mm sized adsorbents by inverse suspension polymerization method.[44] According to the Langmuir model, PAM-LMO resulted in 18.58 mg/g maximum Li^+ adsorption capacity at 293 K and increased to 19.78 mg/g at 318 K, suggesting that the adsorption reaction is endothermic. Column studies, where the selectivity was investigated, showed that the good selectivity towards Li^+ due to the ion-sieve effect. Moreover, in the packed column, no difference in capacity was observed after 30 adsorption-desorption cycles. Both studies suggested that the Li^+ adsorption is intraparticle-controlled process.[43,44] However, it is concluded that the use of PVC resulted in lower mass-transfer coefficient and pore diffusivity compared to PAM. The rationale behind the difference is due to the variance in the hydrophilicity and morphology polymers.

Zhang et al. granulated the H_2TiO_3 with polyethylene glycol (PEG) and poly(ethylene-co-vinyl alcohol) (EVAL) as co-polymer using N,N-dimethylacetamide as solvent by anti-solvent method.[45] Various concentrations of PEH and EVAL were tested for optimized suggestion of adsorbent. According to interconnected porous structure, use of 9% and 7.5% EVAL and PEG concentration were found to be optimum. Adsorption performance was analyzed by using geothermal brine from Southern Tibet and model lithium solutions. The use of model solution yielded maximum Li^+ adsorption capacity of 13.5 mg/g under conditions of pH of 12 and 60 °C, with a contact time was 24 hours, determined by the Langmuir model. On the other hand, use of real geothermal water resulted in 11.8 mg/g at the natural pH of 7.7. Study concluded that after 9 cycles of adsorption-desorption, 91.8% of the initial adsorption capacity was held. Selectivity of Li^+ was investigated in geothermal water and showed good rejection of Mg^{2+}, Na^+, and

K^+ were observed while the separation factor for Ca^{2+} (α_{Ca}^{Li}) was 0.653. However, in desorption studies, it is found that amount of Ca^{2+} desorbed was significantly less than absorbed amount.

Lin et al. studied the granulation of Li_2TiO_3 by PVC as binder.[4] Prior to the granulation, powdery adsorbent Li_2TiO_3 were synthesized by solid-phase calcination and hydrothermal method. It was found that solid-phase calcination method resulted in better performance. The former not only resulted lower in dissolution loss but also showed 2.6 times higher Li^+ adsorption capacity with 16.40 mg/g. Even though the synthesized LTO showed excellent properties, granulation with PVC decreased the adsorption capacity and rate due to the hydrophobic properties of PVC. Thus, it was aimed to improve the adsorption performance of the material by creating polyporous adsorbent with the addition of varying molecular weights of polyethylene glycol (PEG-400 to PEG-10000) in the granulation process. Increase in adsorption capacity were seen with the increase in molecular weight of PEG until the PEG-10000. Thus PEG-6000 was chosen and concentration of it was determined as 24% since addition of more PEG-6000 resulted decrease in stability. The addition of PEG to the material caused the formation of pores on the surface which increased the capacity of the material by preventing the negativity coming from hydrophobicity of PVC. However, exceeding a certain threshold led to loss of stability which was due to an overall decrease in PVC concentration. To conclude, authors suggested the PEG-6000/PVC granulated Li_2TiO_3 which is synthesized by solid-phase calcination method. In the Figure 2.8, difference in the morphology of the addition of PEG-6000 were given.[4] The resulting material was tested in geothermal water obtained from a bore well in the Tibet autonomous region. Adsorbent resulted in the maximum adsorption capacity of 11.35 and 12.84 mg/g at 328.15 K, with the contact time of 12 and 24 hours, respectively. The material showed a 2% decrease in adsorption capacity after 5 adsorption-desorption cycles. Selectivity of Li+ was calculated via separation factor for (α_{Me}^{Li}) and it was calculated as 297.55, 521.28, and 273.58 for Na^+, K^+, and Ca^{2+}, respectively.

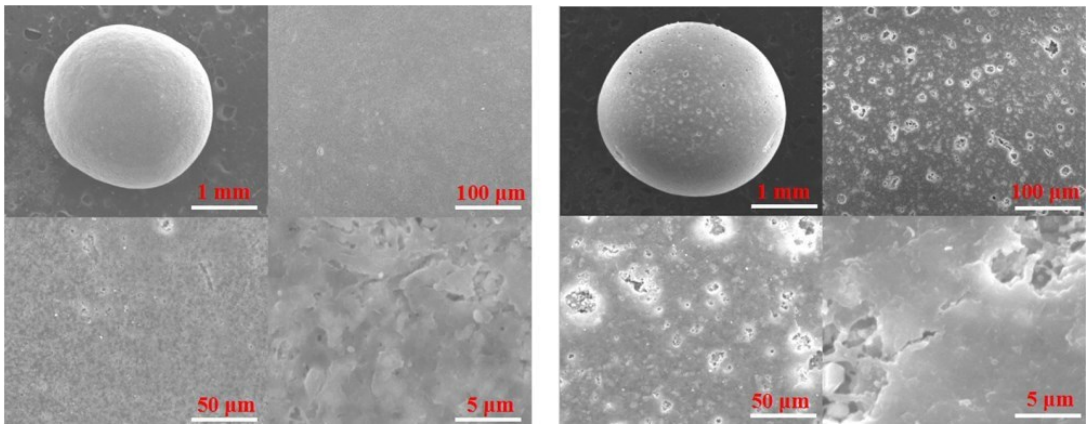

Figure 2.8. SEM images of granulated PVC/HTO where the left is before and the right is after regulating with the PEG-6000[4]

Zhang et al. investigated the performance of the F co-modified $Li_{1.6}Mn_{1.6}O_4$ that is granulated with the mixture of PVC and PAN in N,N-dimethylformamide (DMF) as solvent via anti-solvent method.[46] The study aim was to combine the hydrophobic PVC and hydrophilic PAN to have the advantage of mechanical strength and higher adsorption capacity, respectively. Binder, LIS, and solvent mass ratio of 1:4:13.6 were employed. Furthermore, various binder ratios of PVC to PAN, specifically 1:0, 0.9:0.1, 0.8:0.2, 0.7:0.3, 0.6:0.4, and 0.5:0.5 were experimented. However, when the PAN ratio exceeds 0.7:0.3, granulation slurry for the anti-solvent method fails to form. Remaining ratios were further tested in adsorption experiments. Increasing the PAN ratio resulted in increasing surface pore on the surface of the adsorbent as represented in SEM images in Figure 2.9. These pores eased the target metal ions diffusion into inner portion of the granules thus increasing the adsorption capacity compared to pure PVC adsorbent. According to cycling experiments, it is proved that the increase in PAN ratio, increase in surface pores, yielding instability. Among the experimented ratios, 0.9 to 0.1 PVC to PAN ratio showed the best adsorption capacity and stability. Experimentally 30.04 mg/g of Li^+ adsorption capacity was determined while 31.09 mg/g was calculated according to Langmuir isotherm which is better fit than Freundlich. After 11 cycles of adsorption-desorption, the suggested adsorbent demonstrated a capacity retention of approximately 80%, which closely approached that of pure PVC granules at around 82%, and significantly outperformed the 0.8:0.2 ratio, which resulted in only 45% retention. Authors also experimented with West Taijnar Lake brine to observe selectivity toward

Li^+. The adsorption capacity of Li in real brine measured 17.75 mg/g with the selectivity factors (α_{Me}^{Li}) of 6975, 2711, 943, and 19.71 for Na^+, Mg^{2+}, K^+, and Ca^{2+}, respectively. Indicating that the adsorbent yields high Li^+ selectivity.

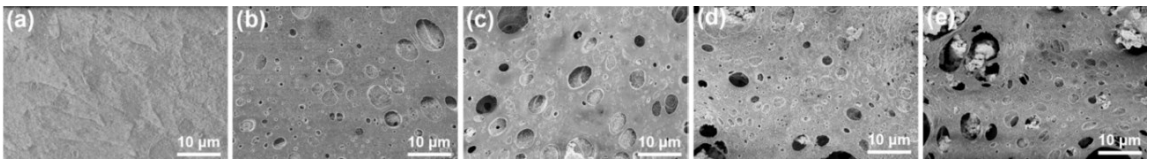

Figure 2.9. Surface images of (a) PVC-HMO-0 (b) PVC/PAN-HTO-10 (c) PVC/PAN-HTO-20 (d) PVC/PAN-HTO-25 (e) PVC/PAN-HTO-30, where the number indicates the percentage of the PAN binder[46]

Table 2.2. Comparison of immobilized adsorbents in the literature

Adsorbent	Binder	Method	Sample	pH	Initial Li^+ Concentration (mg/L)	Adsorption Capacity (mg/g)	Equilibrium Time (h)	Reference
H_2TiO_3	Cellulose Aerogel	Aerogel	LiCl Solution	10.25	50	28.61	36	[42]
H_2TiO_3	PSF	Fiber	Geothermal Water	8.8	25.78	24.57	2	[35]
$H_{1.6}Mn_{1.6}O_4$	PVDF	Fiber	Geothermal Water	8.8	25.78	14.95	2	[47]
$H_{1.6}Mn_{1.6}O_4$	PVA	Foam	LiOH Solution	7.0	7	6.9	24	[30]
H_2TiO_3	PVA	Foam	LiCl Solution	11.0	7	12	12	[32]
HMn_2O_4	PU	Foam	Salt Lake Brine	9	237	1.49	24	[31]
H_2TiO_3	Ceramic Foams	Foam	LiOH Solution	-	2000	21	12	[48]
$H_{1.33}Mn_{1.67}O_4$	AL_2O_3	Granulation	Seawater	-	29.8	9	72	[49]
HMn_2O_4	AAB	Granulation	Seawater	7-8	28.5	8.87	144	[50]
Biogenic HMO	Alginate Beads	Granulation	LiCl Solution	8.5	29.35	24	48	[51]
$H_{1.33}Mn_{1.67}O_4$	AL_2O_3	Granulation	Seawater	-	30	15	72	[52]
HMn_2O_4	PVDF	Granulation	LiOH Solution	-	117.98	19.22	120	[53]
H_2TiO_3	PVC	Granulation	Geothermal Water	12.0	25.58	11.35	12	[4]
$H_4Mn_5O_{12}$	Chitosan	Granulation	Geothermal Water	12.0	25.78	8.98	24	[41]
$H_4Mn_5O_{12}$	Chitosan	Granulation	Geothermal Water	12.0	25.78	11.4	48	[54]
$H_4Mn_5O_{12}$	PVC	Granulation	Simulated Brine	10.0	222	23.47	48	[43]
H_2TiO_3	PVB	Granulation	Simulated Brine	9.2	202	12	5	[55]
H_2TiO_3	EVAL	Granulation	Simulated Brine	7.7	32.11	11.8	24	[45]
$H_{1.33}Mn_{1.67}O_4$	Chitosan	Granulation	LiCl Solution	7-8	30	11.4	168	[56]
$H_4Mn_5O_{12}$	PAM	Granulation	LiCl Solution	10.1	19.6	18.7	20	[44]
H_2TiO_3	PVC	Granulation	LiCl Solution	10.32	200	20.88	2	[57]
Al/F-$H_{1.6}Mn_{1.6}O_4$	PVC/PAN	Granulation	Brine Water	7.1	222.5	11.9	1	[46]
$H_4Mn_5O_{12}$	Epoxy Resin	Granulation	LiCl Solution	6.5	300	30.2	28	[58]
$H_4Mn_5O_{12}$	PVA/CAM	Membrane	LiCl Solution	11	60	23.26	4	[59]
$H_4Mn_5O_{12}$	PVDA	Membrane	LiCl Solution	9	100	27.8	1	[39]
$H_{1.6}Mn_{1.6}O_4$	PVC	Membrane	LiOH Solution	12	150	11.49 mg/m^2	1	[38]
$H_{1.6}Mn_{1.6}O_4$	PAN	Membrane	Simulated Brine	9.2	50	18.1	12	[60]
$H_{1.6}Mn_{1.6}O_4$	PAN	Nanofiber	LiCl/LiOH Solution	11.0	35	10.3	24	[34]
H_2TiO_3	PAN	Nanofiber	Li^+ Solution	11.0	70	32	24	[36]
HMn_2O_4	Agar	SIF	LiOH Solution	13.0	2395	20.9	24	[61]

CHAPTER 3

METHODOLOGY

3.1. Materials

The chemical used in this study were given in Table 3.1. Also, Geothermal water used in the experiments was collected from Germencik Power Plant (Aydın, Türkiye) and pH and composition of the geothermal water given in Table 3.2.

Table 3.1. List of chemicals

Chemicals	**Chemical Formula**	**Manufacturer**
Hydrochloric Acid	HCl	Merck
Lithium Carbonate	Li_2CO_3	Merck
Lithium Chloride	LiCl	Merck
N,N-Dimethylformamide	C_3H_7NO	Merck
Polyacrylonitrile	$(C_3H_3N)_n$	Merck
Polyvinyl Chloride	$(C_2H_3Cl)_n$	Merck
Sodium Chloride	NaCl	Merck
Sodium Hydroxide	NaOH	Tekkim Kimya
Sulfuric Acid	H_2SO_4	Merck
Titanium Oxide	TiO_2 (Anatase)	Merck

Table 3.2. Composition of geothermal water used in this work

pH	**Li^+ (mg/L)**	**Na^+ (mg/L)**	**K^+(mg/L)**	**Mg^{2+} (mg/L)**	**Ca^{2+} (mg/L)**
6.6	8.50	1211.66	75.70	2.47	23.25

3.2. Synthesis of the Adsorbent

3.2.1. Synthesis of the Li_2TiO_3

For the synthesis of powder adsorbent, Li_2TiO_3, following procedure were applied[23]: Anatase type TiO_2 and Li_2CO_3 were mixed by considering stoichiometric ratio of Ti and Li. 15 grams of TiO_2 and 13.9 grams of Li_2CO_3 were mixed in a mortar and pestle and grounded for 20 minutes to decrease the particle size of the reagents and to mix the powder reagents homogenously. Mixture was transferred into a crucible porcelain and heated in a forced circulation oven up to 700 ℃ with the heating rate of 6 ℃/min then maintained at 700 ℃ for 4 hours. Once the resulting powder (Li_2CO_3) cooled down, grounded with a mortar and pestle to reduce the particle size of the product.

3.2.2. Granulation of the Li_2TiO_3 with the PVC/PAN Composite

For the industrialization of the powdery adsorbent, it is granulated with the solvent phase conversion method[46]. 292 mL of N,N-dimethylformamide (DMF) was poured into a beaker. Then 18 grams of PVC and 2 grams of PAN were slowly added into the DMF, under vortex, respectively. The solution was mixed under vortex until it is free of bubbles and looks homogeneous. 80 grams of synthesized Li_2CO_3 were slowly added into the vortex of the clear solution and mixed until homogeneous white slurry obtained. By using syringe, slurry was transferred into the distilled water, drop by drop. Each droplet of slurry forms a spherical shape as it contacts the distilled water. Formed spherical adsorbents, (PVC/PAN-LTO), then transferred into a filter paper and washed with distilled water until the precipitate solution′s conductivity decreased. Lastly, adsorbents were dried in a forced circulation oven for 12 hours at 50 ℃.

3.2.3. Delithiation of PVC/PAN-LTO

In order for the material to retain lithium, adsorbent should be activated by stripping the lithium and exchange with hydrogen ion. 250 mL of 0.25 mol/L HCl solution were prepared to react with a gram of PVC/PAN-LTO to transform the adsorbent to PVC/PAN-HTO. The ion-exchange reaction was conducted in shot bottles and shaken in a multifunctional water bath for 12 hours at 25 °C and 180 rpm. Once the reaction was completed, media were transferred to a filter and washed with distilled water until the pH of 7 reached in the precipitate. Lastly, adsorbents were dried in a forced circulation oven for 12 hours at 50 ℃.

3.3. Characterization of Adsorbent

Surface morphology and structure of the samples was investigated by Scanning Electron Microscope (ZEISS EVO10). Brunauer-Emmett-Teller (BET) surface area and Barrett-Joyner-Halenda (BJH) pore volume of the samples were determined using Micromeritics Gemini V analyzer. To analyze the bond structures, IR spectra in the range of 4000 to 400 cm^{-1} were conducted using Perkin Elmer UATR-FT-IR device (4 cm^{-1} resolution, 20 scans per sample). Lastly, crystalline structure of the material were determined by XRD (Philips X'Pert Pro) using Cu-Kα radiation as X-ray source with the characterization parameters of 45 kV generator voltage, 40 mA tube current, 1.54056 Å wavelength, and the scanning range of $5 < 2\theta < 80$.

3.4. Adsorption Studies

Performance of the synthesized PVC/PAN-HTO were analyzed by performing batch adsorption experiments using 10 ppm lithium stock solution and geothermal water obtained from Germencik Power Plant. The study examined the effect of adsorbent

dosage, pH, initial lithium concentration and temperature, and cycling performance. Unless specified otherwise, batch adsorption studies were conducted in 50 mL solution for 24 hours at 25 ℃ and 180 rpm in a closed glass bottles with the volume of 75 mL. The operating time, temperature, and shaking rate were set by using multipurpose water baths shaker (Faithful FWS-30).

3.4.1. Effect of pH

10 ppm model lithium solution's pH were adjusted between 2 to 12 to examine the effect of pH. Since Na is the most abundant ion in brine waters and Cl is too large to fit in vacancies on adsorbent, NaOH and HCl were used for pH adjustment.
Additionally, after the batch adsorption, final values of pH were measured for each flask. Initial pH to ΔpH were plotted to determine the point of zero charge (PZC). PZC was the value where the ΔpH is zero and describes the net charge of total particle surface equals to zero. Calculation of ΔpH is given in the Equation 3.1

$$\Delta pH = Initial\ pH - Final\ pH \qquad 3.1$$

3.4.2. Effect of Adsorbent Dosage

To determine the optimal amount of adsorbent required for the recovering lithium from 10 ppm lithium model solution and geothermal water, ranging amounts of adsorbents from 1 g/L to 10 g/L were used in 50 mL solution.

3.4.3. Effect of Initial Lithium Concentration and Temperature

Initial concentration of 5, 10, 25, 50, 75, and 100 ppm lithium stock solutions were prepared and conducted batch adsorption in temperatures of 25, 40, 55 ℃. Hence, the effect of lithium concentration, effect of temperature, and adsorption isotherms can be determined.

3.4.4. Desorption Performance

Adsorbent (PVC/PAN-HTO) were saturated with 100 ppm lithium model solution and regeneration performance were analyzed by using 0.10, 0.25, and 0.50 molarity of HCl, H_2SO_4, and NaCl. Equation 3.2 were used to calculate desorption capacity where C_0 and C_f are initial concentration and final concentration, respectively.

$$Desorption\ rate\% = \frac{C_f}{C_0} * 100 \qquad 3.2$$

3.4.5. Cycling Performance

To understand the reusability of the adsorbent, a series of coupled adsorption and desorption experiments were conducted. Firstly, delithiation of 1 gram of PVC/PAN-LTO was performed in 250 mL 0.25 mol/L HCl. PVC/PAN-HTO was washed with distilled water until the pH of the precipitate neutralized and then dried for 12 hours at 50 ℃. Subsequently, adsorption in 250 mL of 10 ppm model lithium solution was conducted. After the adsorption, adsorbent was washed with distilled water until the conductivity decreased and dried for 12 hours at 50 ℃. This procedure was counted as one cycle.

3.4.6. Adsorption Kinetics

To reveal the adsorption kinetics of the suggested adsorption, series of kinetic studies were carried out at three different temperatures (25, 40, 55 °C). Adsorbent dosage of 4 g/L were used in 750 mL of 10 ppm lithium containing solution and geothermal water at rotational speed of 180 rpm. Samples were taken at the time of 0, 5, 10, 15, 20, 30, 45, 60, 90, 120, 180, 240, 360, 480, and 1440 minutes.

Moreover, pseudo first order and pseudo second order reaction kinetic parameters were calculated using the Equation 3.3 and Equation 3.4.[62] Least-squares regression approach were used and the slope and intercepts of the plot of $\ln(q_e - q_t)$ versus t and t/q_t versus t were used. In the equations, q_t (mg/g) and q_e (mg/g) is the amount of lithium adsorbed at the specified time and at equilibrium, respectively. k_1, k_2, and t are the first order rate constant, second order rate constant, and time (min), respectively.

$$\ln(q_e - q_t) = \ln(q_e) - k_1 t \qquad 3.3$$

$$\frac{t}{q_t} = \frac{1}{k_2 q_e^2} + \frac{t}{q_e} \qquad 3.4$$

3.4.7. Adsorption Isotherms

The relationship of absorbing lithium ions and highest adsorption capacity were examined by the isotherms. Two most common adsorption isotherm models, Langmuir and Freundlich equations, were employed. As mentioned in Section 3.4.3, adsorption performed with varying initial concentrations of lithium (5 to 100 ppm) performed with 4 g/L adsorption dosage. Results of the experiment were used to derive the adsorption isotherms according to the Equation 3.5 for Langmuir[63] and Equation 3.6 for Freundlich[64] using the least-squared regression, respectively. In equations q_e, q_{max}, K_L, C_e, K_F and n stands for equilibrium adsorption capacity (mg/g), maximum adsorption capacity (mg/g),

constant of Langmuir isotherm model (L/mg), and constants of Freundlich isotherm model.

$$q_e = q_{max} \left(\frac{K_L C_e}{1 + K_L C_e} \right) \quad 3.5$$

$$q_e = K_F C_e^{\frac{1}{n}} \quad 3.6$$

3.4.8. Adsorption Thermodynamics

To be able to calculate standard Gibbs free energy change ($\Delta G°$), standard entropy change ($\Delta S°$), and standard enthalpy change ($\Delta H°$) thermodynamic calculations were conducted by using the initial concentration data from Section 3.4.3. Adsorption of varying initial concentrations of model lithium solution (5 to 100 ppm) at temperatures of 25, 40, and 55 °C were conducted to derive K_L value at Section 3.4.7 to be able to use in the Equation 3.7 which is to calculate standard Gibbs free energy change. In the following equation T, R and K_L are temperature (K), gas constant (J/mol.K), and Langmuir isotherm constant (L/mg), respectively. Calculated value of $\Delta G°$, explains the adsorption behavior whether it is spontaneous or not. If the value is negative at experimented temperature, adsorption reaction rakes place spontaneously.

$$\Delta G° = -RT \ln K_L \quad 3.7$$

Standard entropy change ($\Delta S°$) and standard enthalpy change ($\Delta H°$) were calculated by using Van't Hoff equation as described in the Equation 3.8.[65] Linear equation analogy was made to the Van't Hoff equation and by plotting the $\ln K_E$ versus $1/T$, $\Delta S°$ and $\Delta H°$ were determined. The value of K_E is in the unit of L/mg and should be dimensionless in Van't Hoff equation, hence K_E were calculated by transformation of K_L

which was obtained from fitted isotherm model to utilize in Equation 3.9.[66] In Equation 3.9 MW_{Li^+}, $[Ion]^0$, and γ stands for molecular weight of lithium ion, standard concentration of the ion (1 mol/L), and activity coefficient, respectively.

$$\ln K_E = \frac{\Delta S°}{R} - \frac{\Delta H°}{RT} \quad 3.8$$

$$K_E = (1000 * K_L * MW_{Li^+}) * [Ion]^0/\gamma \quad 3.9$$

3.4.9. Measurement of Lithium and Competitor Ions

Since geothermal water contains competitor ions of Na^+, Mg^{2+}, K^+, and Ca^{2+} rejection of those ions is crucial. All the lithium and competitor ion concentrations were analyzed via ICP-OES (Agilent Technologies, 5110). Necessary dilutions were performed to measure precisely according to instrument's specifications for each ion. To be able to calculate lithium recovery (r) and adsorption capacity (q), Equation 3.10 and 3.11 were used where C_0, C_f, V, and m are initial concentration, final concentration, volume of solution containing solute, and mass of the adsorbent, respectively.

$$r = \frac{C_0 - C_f}{C_0} * 100 \quad 3.10$$

$$q = V\left(\frac{C_0 - C_f}{m}\right) \quad 3.11$$

Moreover, to calculate the selectivity of the adsorbent toward Li^+ ion, separation factor (α_{Me}^{Li}) were calculated according to Equation 3.12 and 3.13 where $K_{d(Me)}$ is the distribution coefficient for a metal ion , C_0, C_e, V, and m are initial concentration of metal ion, equilibrium concentration of metal ion, volume of the test sample, and mass of

adsorbent, respectively. The separation factor was determined by the ratio of distribution factor of two metal ions. The factor, α_{Me}^{Li}, demonstrates the lithium selectivity to other metal ion (Me = Na^+, Mg^{2+}, K^+, or Ca^{2+}) and the high value means more selective lithium recovery.[67]

$$K_{d(Me)} = \frac{(C_0 - C_e)V}{mC_e} \quad 3.12$$

$$\alpha_{Me}^{Li} = \frac{K_d(Li)}{K_d(Me)} \quad 3.13$$

CHAPTER 4

RESULTS AND DISCUSSION

4.1. Characterization Results

In this following sub-section characterization results of the suggested adsorbent was provided.

4.1.1. FT-IR Analysis

FT-IR spectra of the PVC/PAN, LTO, PVC/PAN-LTO, and PVC/PAN-HTO were presented in Figure 4.1. The peaks between ~3000-2850 cm^{-1} for all spectra except LTO stands for C-H stretching vibration from the polymer matrix. The peaks at the ~2245 cm^{-1} and ~1450 cm^{-1} were the characteristic peaks for C≡N and N≡O bonds of the PAN polymer, respectively. Also, in the spectra of PVC/PAN, the fluctuation in the spectra between ~700-550 cm^{-1} was the representation of the halogen carbon stretching which is C-Cl stretching of the PVC polymer. The expected Ti-O bond stretch for the LTO were presented as peaks at the ~750 cm^{-1} and metal-oxygen stretch (Ti-O-Ti or Li-O) was the reasoning of the peaks around ~750-450 cm^{-1}. Those metal-oxygen stretch peaks were also presented in spectra of the PVC/PAN-LTO and PVC/PAN-HTO as these materials consisted of LTO, as well. The peak at ~1550-1400 cm^{-1} interpreted as the $LiCO_3$ impurities which remained from the synthesis of the material. Lastly, unique peak around the ~850 cm^{-1} for PVC/AN-LTO interpreted as the specific interactions or bonding between the polymer matrix and LTO.

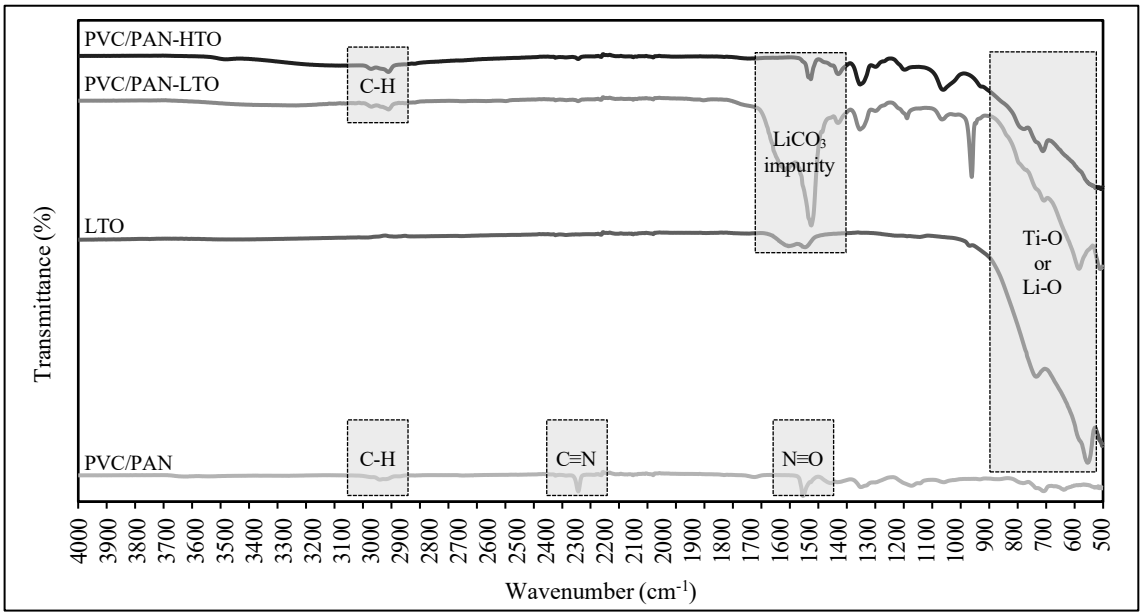

Figure 4.1. FT-IR spectrum of PVC/PAN, LTO, PVC/PAN-LTO, and PVC/PAN-HTO

4.1.2. BET Analysis

Surface area and the pore volume are crucial parameters for adsorbents as these morphologic parameters affect adsorption and desorption properties. BET and Langmuir surface areas and pore volume distribution and total prove volume were given in Table 4.1. LTO and mixed PVC/PAN have similar BET surface area of 4.4652 and 4.4503 m^2/g, respectively. However, after the granulation BET surface remarkably increased by approximately 224%, due to forming 3D structured spherical material. Moreover, delithiation of the PVC/PAN-LTO resulted in a further increase in BET surface area by 47.3% which was due to stripping of Li^+ ions by replacing them with H^+ ions. According to BJH pore distribution only micro and mesopores were detected and not macropores were determined. This finding is consistent as the adsorbent has the ion-sieve effect specifically tailored for the smallest metal ion, lithium. Granulation of the powder adsorbent resulted in 116.8% increase in total pore volume and 81.6% further increase after delithiation. In granulation, micropores distribution were increased to 12.60% from 4.84%, which was then decreased below powder adsorbent by 2.59% after delithiation

process. Ion-exchange of Li^+ with H^+, which is a smaller ion, was the reasoning of the increase in the mesopores.

Table 4.1. Pore distribution, pore volume, and BET surface area of granule matrix (PVC/PAN), powdery adsorbent (LTO), granule adsorbent (PVC/PAN-LTO), and active granule adsorbent (PVC/PAN-HTO)

Material	Pore Volume (%)		Total Pore Volume	BET Surface Area
	Micropores (<2 nm)	Mesopores (2-50 nm)	(cm^3/g)	(m^2/g)
PVC/PAN	5.12	94.88	0.004375	4.4503
LTO	4.84	95.16	0.004176	4.4652
PVC/PAN-LTO	12.60	87.40	0.009054	14.4807
PVC/PAN-HTO	2.59	97.41	0.016440	21.3275

4.1.3. XRD Analysis

The XRD diffractograms of PVC/PAN mixture (0.9:0.1 mass ratio), LTO, PVC/PAN-LTO, and PVC/PAN-HTO were presented in the Figure 4.2. The diffractogram of LTO agreed with the XRD diffractogram reported by Chitrakar et al., which served as the basis for the synthesis procedure of the powdery adsorbent.[23] This finding suggest that the material was correctly synthesized. The granulation of the LTO with the mixture of PVC/PAN resulted in a decrease in the crystallinity as expected (Figure 4.2-e), since the polymeric mixture was in amorphous structure which were also proven by the XRD diffractogram of it. As also can be seen from Figure 4.2-e, intensity of the peaks were significantly decreased when the LTO was granulated with the PVC/PAN, but the peaks are still sharp. Since the XRD is a surface characterization technique (up to 2 nm below surface), this evidence suggest that LTO still existed on the surface of the granulated adsorbent while the polymeric matrix was effectively coated the surface. Thus, the granulation were successfully carried out. Lastly, XRD pattern of the PVC/PAN-HTO was similar to PVC/PAN-LTO, which was obtained after delithiation, as shown in the Figure 4.2-f. Disappearance of the peak around the 2θ value of 44° can be interpret as the change on the surface structure due to ion exchange of the lithium with hydrogen.

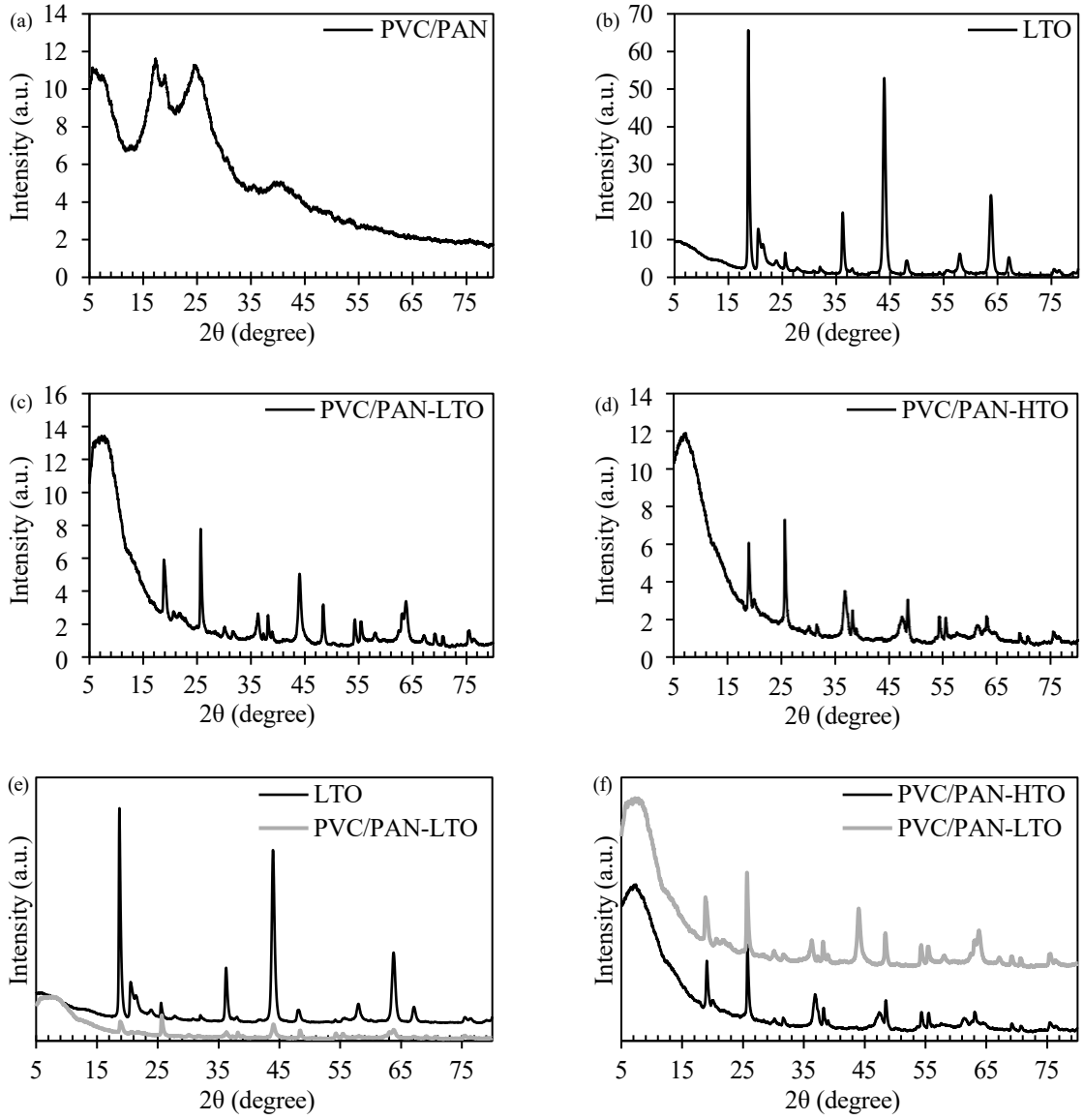

Figure 4.2. XRD diffractograms of (a) PVC/PAN, (b) LTO, (c) PVC/PAN-LTO, and (d) PVC/PAN-HTO; and comparison of the diffractograms of (e) granulation and (f) delithiation

4.1.4. SEM Analysis

In Figure 4.3, SEM images of the PVC/PAN mixture, LTO, PVC/PAN-LTO, and PVC/PAN-HTO were presented. Granulation of the powder LTO with PVC and PAN formed smooth layer of polymer on surface. Thus, surface of the granule was smoother

that the powder adsorbent. In the Figure 4.3-c and -d, pores of the material can be seen where the water will pass through to attract with the LTO inside of the granule. Increase in the BET surface area, which were described in Section 4.1.2, was correlated with the surface morphology of the granulized adsorbent. SEM analysis also results that the coating of the LTO with the polymer was successful according to the morphology changes of the surface.

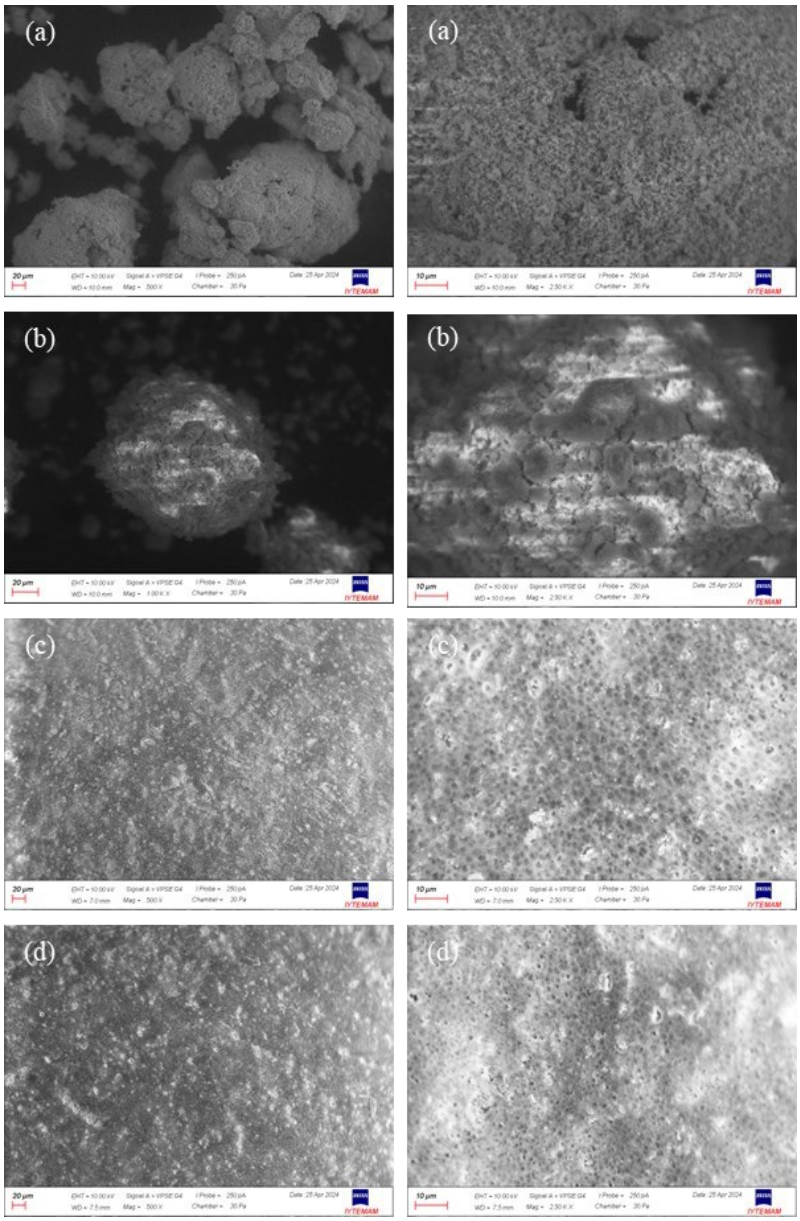

Figure 4.3. SEM images of (a) PVC/PAN, (b) LTO, (c) granule PVC/PAN-LTO, and (d) granule PVC/PAN-HTO; right 1000x and left 2500x magnification

4.2. Adsorption Studies

The adsorption performance of the suggested material (PVC/PAN-HTO) was evaluated via batch experiments and results were given in this section. Model 10 ppm lithium solution was used for effect of pH, adsorbent dosage, initial concentration, desorption, cycling, and kinetic while geothermal water was used for adsorbent dosage and kinetic studies.

4.2.1. Effect of pH

By using 10 ppm model lithium solution, various pH values of 2 to 12 were evaluated with 4 g/L adsorbent dosage as rule of thumb. The results of the experiment were given in the Figure 4.4 and as seen, lithium recovery is only possible in the alkaline media. In acidic media adsorbent were continued to release the remaining Li^+ ions to the solution. This finding was expected since to activate the material, for the delithiation, HCl were used. However, the finding proved that the adsorbent still consists of Li^+ ions even after the delithiation. At pH value of 8, lithium recovery was seen as 5.68% and significantly increased to 96.67% when the pH is 12.

During the adsorption period, adsorbent releases H^+ ions to the media to exchange with Li^+ ion. Thus, through the adsorption period solution becomes more acidic. As seen from the Figure 4.4, in the acidic media Li^+ removal from adsorbent to media occurs rather than Li^+ recovery from solution to absorbent. Reasoning can be explained according to Le Chatelier's principle as the mechanism of the ion-exchange reaction which was described in the Equation 4.1. Also, Na^+ ions, existing from NaOH for pH adjustment, function as buffer for transformation into acidic environment and allows to adsorption process continue.

$$Li_2TiO_3 + 2H^+ \leftrightarrow H_2TiO_3 + 2Li^+ \qquad 4.1$$

As the highest Li^+ recovery was obtained at pH of 12 with 96.67% recovery, subsequent experiments were conducted at pH of 12 for the model solution. Since geothermal waters consist of other ions such as Na^+, K^+, Mg^{2+}, and Ca^{2+}, adjusting pH to alkaline media in model lithium solution yields more accurate and optimal results.

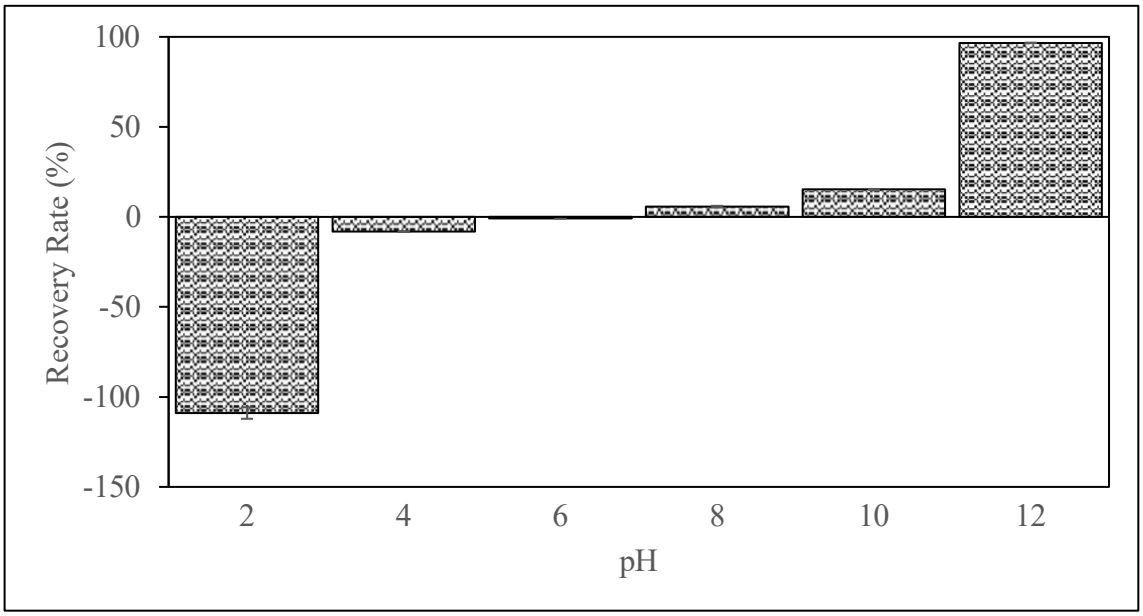

Figure 4.4. Effect of pH on the lithium recovery rate (C_0 = 10 mg/L, T = 25 °C, and AD = 4 g/L)

Additionally, the point of zero charge (PZC) was determined by using pH drift method. As illustrated in the Figure 4.5, pH_{PZC} were identified as 6.03 according to relevant root of the trendline with the R-square of 0.98. Above the pH value of pH_{PZC}, surface of the adsorbent is negatively charged, and vice versa. Hence, above the value of pH_{PZC}, adsorbent attracts the cations ions to the surface while repelling the anions. Lithium, a cation in solution, was repelled at acidic values of pH by the positively charged surface of the adsorbent thus little to no recovery rate were achieved as seen in Figure 4.4.

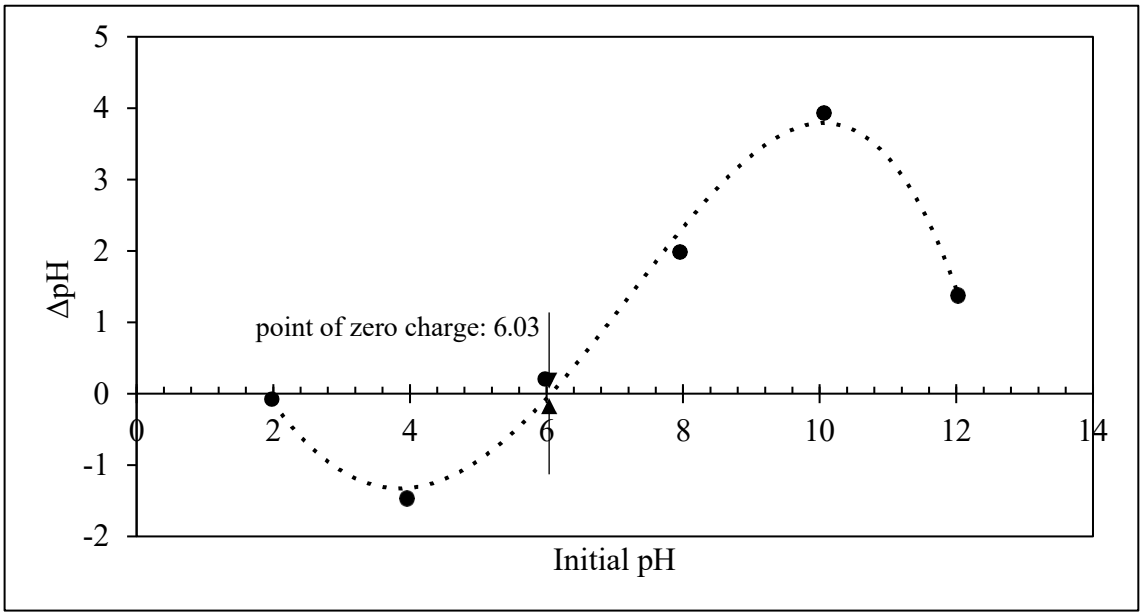

Figure 4.5. Plot for determining point of zero charge for PVC/PAN-HTO (C_0 = 10 mg/L, T = 25 °C, and AD = 4 g/L)

4.2.2. Effect of Adsorbent Dosage

Mass of adsorbent used per liter of lithium containing solution were investigated for 10 ppm model lithium solution with pH of 12, geothermal water, and geothermal water with pH of 12.

The result of the effect of adsorbent dosage (AD) for model lithium solution presented in Figure 4.6. Increasing the mass of adsorbent to 4 g/L increased the lithium recovery gradually up to 98.27%. Furter increase in the dosage insignificantly increased the recovery rate up to 98.45% at 8 g/L. Thus, 4 g/L adsorbent dosage were seen to be economically optimum for the tested adsorption conditions.

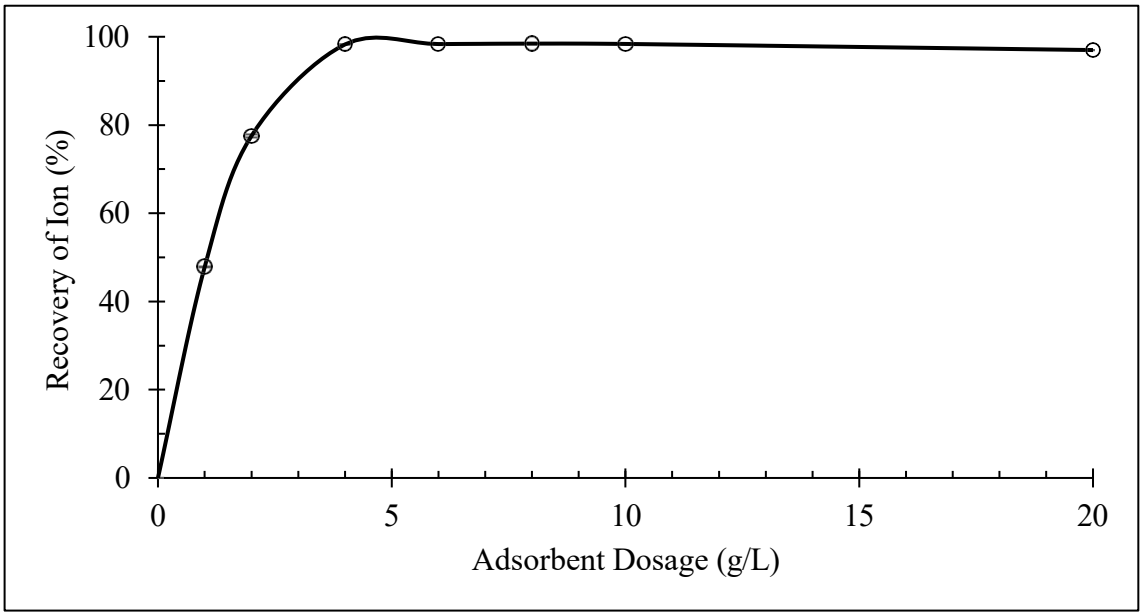

Figure 4.6. Effect of adsorbent dosage on lithium recovery on model lithium solution (C_0 = 10 mg/L, T = 25 °C, and pH = 12)

Dosage of adsorbent on Li^+ recovery was also investigated in geothermal water to understand the effects of competitor ions and to compare with model solution. Recovery of lithium increased progressively up to 91.63% at 4 g/L adsorbent dosage as shown in Figure 4.7. Equilibrium was nearly reached at 4 g/L since increase of dosage to 20 g/L resulted in 93.79% lithium recovery which is insignificant. Selectivity of toward Li^+ ion was remarkably high. In order to quantitatively analyze the selectivity, selectivity factor for each ion respectively to lithium was calculated and given in the Table 4.2. The selectivity order of the adsorbent under the experimented conditions at 4 g/L dosage was $Li^+ >> K^+ > Na^+ > Ca^{2+} > Mg^{2+}$.

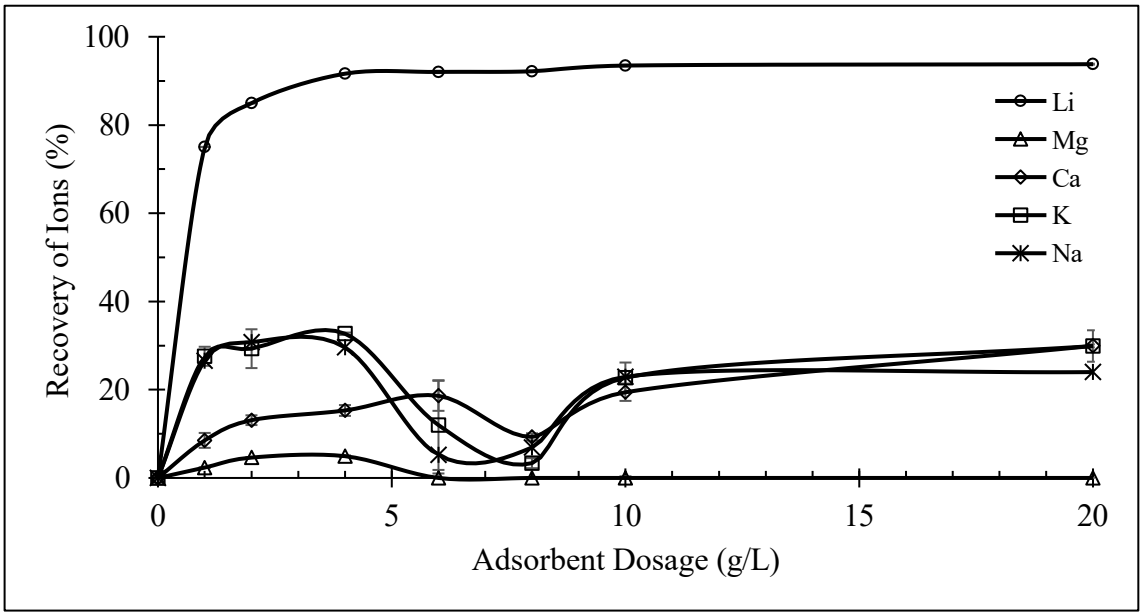

Figure 4.7. Effect of adsorbent dosage on lithium recovery on geothermal water (T = 25 °C)

Lastly, geothermal water's pH was adjusted to 12 for the adsorbent dosage investigation. The aim was to determine whether it would be possible to reduce the dosage by increasing the pH, as in model lithium solution. As seen in Figure 4.8, lithium recovery was 97.54% at 4 g/L while almost complete lithium recovery was achieved at 6 g/L with 99.73% recovery. However, increasing pH also resulted in 84.42%, and 15.69% recovery adsorption of Mg^{2+} and K^{+} ion at 4 g/L dosage, respectively. On the other hand, high pH value resulted in complete rejection of other competitor ions, Na^{+} and Ca^{2+}. The result of selectivity factor calculation for each ion respectively to lithium were given in Table 4.2. The selectivity order of the adsorbent under the experimented conditions at 4 g/L dosage was $Li^{+} > Mg^{2+} >> K^{+} > Ca^{2+} > Na^{+}$. Selectivity of Mg^{2+} exceeded calcium selectivity when the pH of geothermal water was increased to 12.

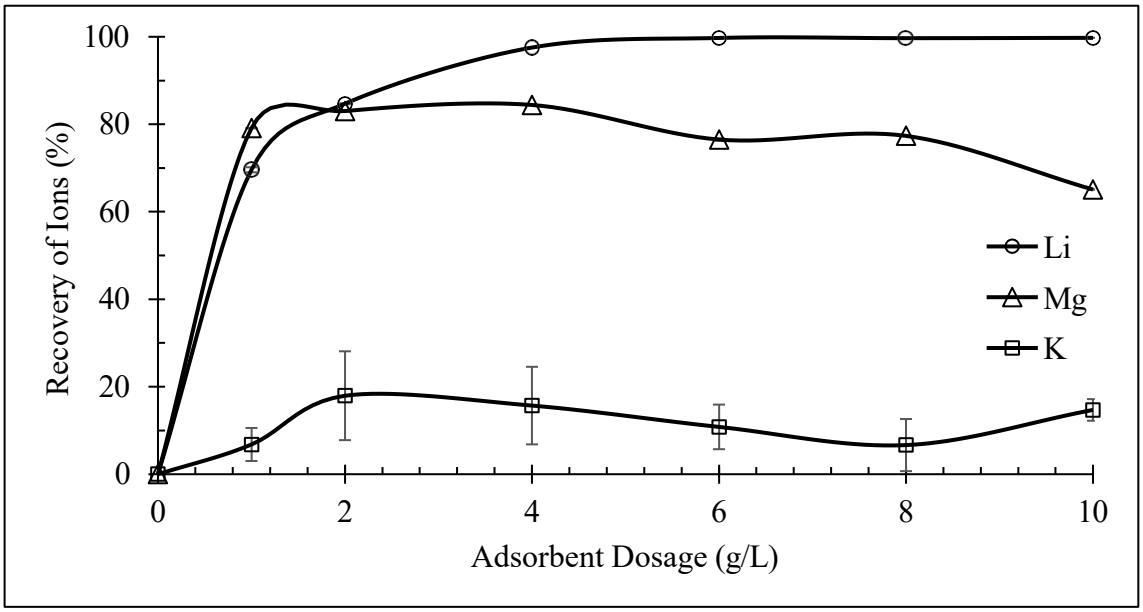

Figure 4.8. Effect of adsorbent dosage on lithium recovery on geothermal water (T = 25 °C and pH = 12)

Table 4.2. Separation factors of lithium against Na, K, Mg, Ca (T = 25 °C, AD = 4 g/L)

Solution	α_{Li}^{Li}	α_{Na}^{Li}	α_{K}^{Li}	α_{Mg}^{Li}	α_{Ca}^{Li}
Geothermal Water	1.00	26.07	22.55	210.88	60.66
Geothermal Water (pH = 12)	1.00	529.76	213.40	7.33	447.86

4.2.3. Effect of Initial Lithium Concentration and Temperature

Ranging from 5 ppm to 10, 25, 50, 75, and 100 ppm initial lithium concentration were examined while all concentrations were cross investigated at the temperature of 25, 40, and 55 °C. All concentrations were adjusted to pH of 12. The results of the experiment were depicted in Figure 4.9.

Increase in the temperature increases the lithium recovery in every tested scenario especially at lower concentrations. This behavior suggests endothermic adsorption, experimentally. Even though the recovery rate of lithium is the highest at lower concentrations, adsorption capacity is the highest at higher concentrations as shown in Figure 4.9. The highest adsorption capacity was experimentally calculated as 6.45 mg/g

at 100 ppm lithium solution at 25 °C which is due to the availability of the abundant Li^+ ions in the solution for adsorbent. Results of this experiment were also used for extracting adsorption isotherms and adsorption thermodynamics which were explained in Section 3.4.7 and Section 3.4.8, respectively.

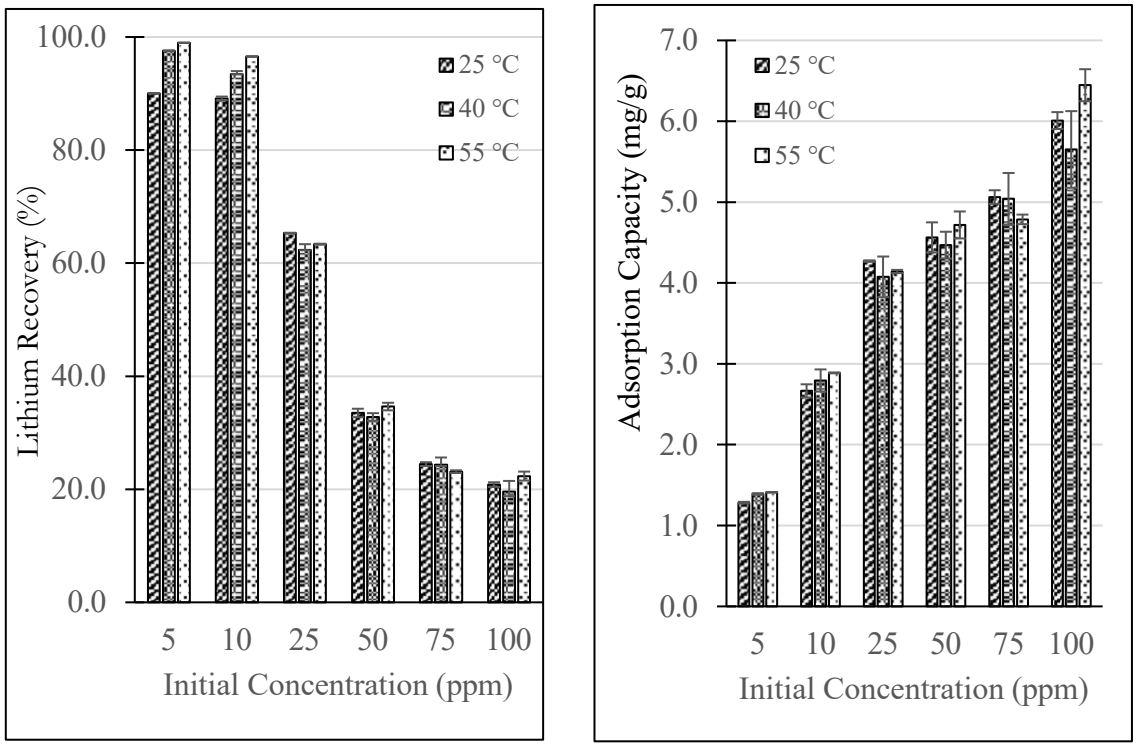

Figure 4.9 Initial concentration and temperature dependency of (left) lithium recovery rate and (right) adsorption capacity (AD = 4g/L)

4.2.4. Desorption Performance

The objective of the desorption study is to analyze the retrievable lithium after adsorption. Batch adsorption studies were included lithium recovery in percentage from lithium containing solution to adsorbent. Desorption study covers the ion-exchange of recovered lithium from adsorbent to eluent. The eluent then can be used for recovery of lithium salts, by evaporation or such purification steps which is not in the scope of this study.

Adsorbent was saturated with 100 ppm lithium solution at pH of 12 in a batch adsorption. HCl, H_2SO_4, and NaCl were used as the eluent and molarity of 0.10, 0.25, and 0.50 were tested.

The percentage of the desorbed lithium to the eluent from adsorbent were given in Figure 4.10. Results indicated that diprotic acid H_2SO_4 resulted in a higher desorption rate than HCl which is aprotic. Desorption rate of 88% achieved with 0.1 M H_2SO_4. Also, the desorption rate achieved in molarity of 0.25 and 0.50 of H_2SO_4 were identical and was 95%. Hence, increasing the acid strength did not result in higher desorption rate which makes the use of higher acid molarity unnecessary. On the other hand, HCl resulted in the same desorption percentages at 0.10 and 0.25 molarity with 82% while 0.50 molarity resulted 90% desorption rate. Thus, increasing the molarity of HCl up to a level between 0.25 to 0.50 is unnecessary in terms of Li^+ desorption rate. Lastly, increase in molarity from 0.10 to 0.25 and 0.50 increased the desorption rate by 15% to 24% and 32% when NaCl were used as eluent. This finding gives a rough understanding of competing ion Na^+ selectivity to Li^+ selectivity. Overall, lithium desorption efficiency of the adsorbent proven to be promising. Remarkable desorption rates up to 95% can be achieved when harsh acid conditions were applied and noteworthy rates such as 82% can be achieved when mild conditions considered.

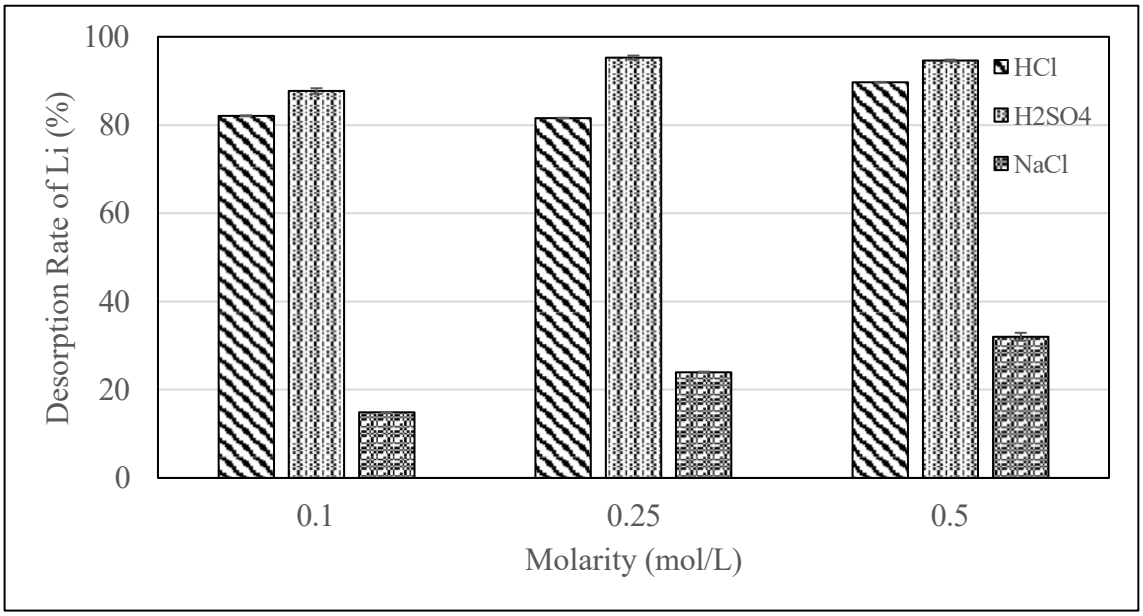

Figure 4.10. Desorption of Li from adsorbent using different eluents at different molarities (T = 25 °C)

To be able to have an insight into the reusability of the adsorbent, titanium presence was investigated in the eluent. As shown in Figure 4.11, significant presence of Ti was observed when an acid was used as the desorption eluent while no Ti concentration was detected when NaCl was used. Even though no difference in lithium desorption was observed at 0.10 and 0.25 molar HCl eluent, leach of Ti was four-fold. Also, three-fold presence of Ti was observed at 0.50 M compared to 0.25 molar HCl. On the other hand, diprotic acid (H_2SO_4) of 0.10 and 0.50 molarity were used 115 to 682 mg/L Ti concentration presence was observed which is extreme. Since lithium desorption rates were high at both acids, use of diprotic acid proven to be redundant in terms of reusability of the adsorbent.

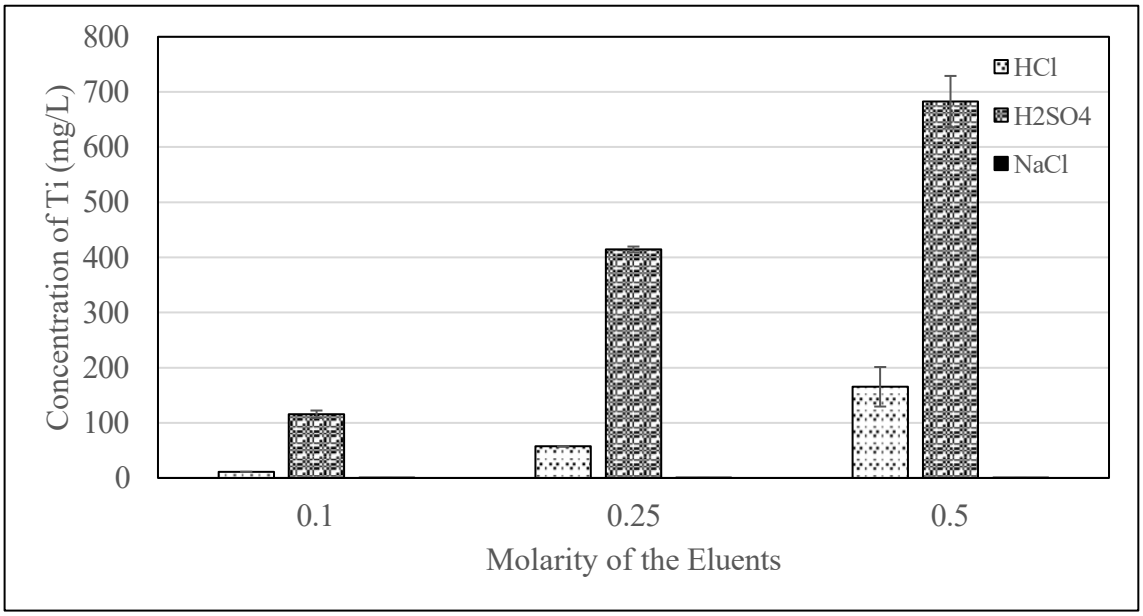

Figure 4.11. Presence of titanium in eluent solutions

4.2.5. Cycling Performance

In the desorption process leaching of titanium into the lithium rich solution was detected in Section 4.2.4. Therefore, stability of the suggested adsorbent, PVC/PAN-HTO, was considered. Three consecutive adsorption-desorption cycles have been performed with model lithium solution after the material was activated by delithiation process. The relative decrease in lithium recovery rate at the third cycle compared to first was %2.07. The lithium recovery rate of the first adsorption was 96.8% while the second and third adsorption resulted in 96.4% and 94.8%, respectively. This finding suggests that the material is suitable for reuse. However, to determine the lifetime of the material more cycles should be performed.

4.2.6. Adsorption Kinetics

Kinetic studies were carried out to understand the contact time, effect of competitor ions with respect to time, and adsorbent performance. Experiment of 10 ppm lithium model solution and geothermal water have been used at temperatures of 25, 40, and 55 °C. Also, geothermal water with a pH of 12 was tested at 25 °C to understand whether it would create positive difference in kinetic of the adsorption rate, as it did in the model lithium solution.

Kinetic study results of 10 ppm lithium model solution at different temperatures were given in Figure 4.12. The study proved that the temperature is an important factor to achieve faster lithium adsorption. Adsorption behavior for each temperature were decaying exponential functions with different preexponential factors. Faster adsorption occurs at higher temperatures. The Li^+ uptake equilibrium of was reached at 8^{th} hour to the same recovery rate for temperatures of 25 °C and 40 °C while the equilibrium was reached at 6^{th} hour for the 55 °C due to the faster adsorption kinetic. Even though a slight increase in lithium recovery was seen at the temperature of 25 °C up to 24^{th} hour, the increase was insignificant. At each temperature tested, equilibrium adsorption capacity converged to around 2.60 mg/g.

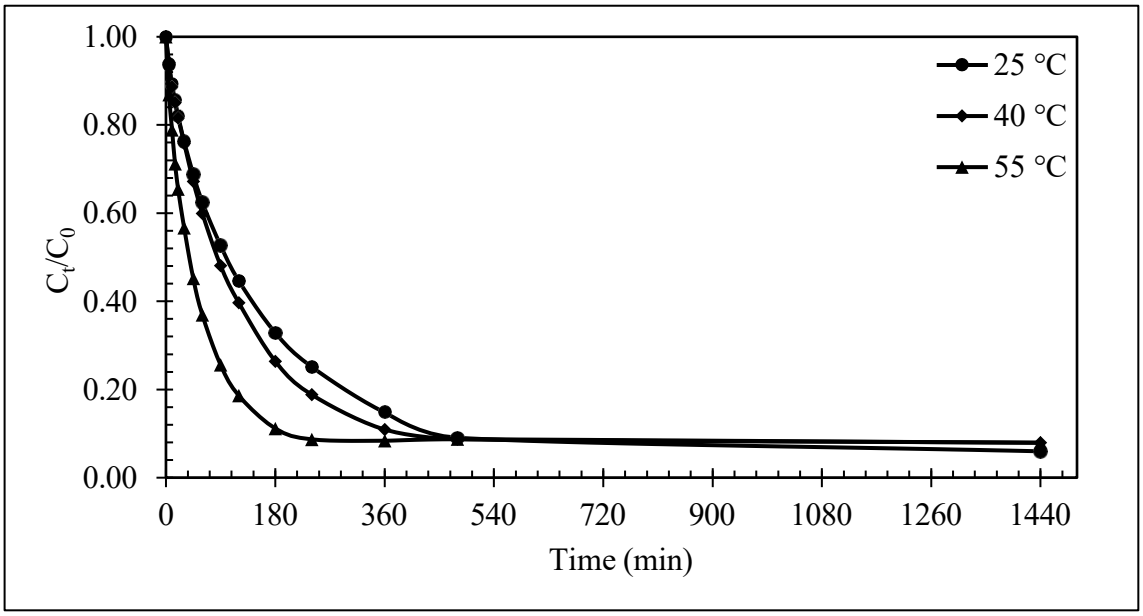

Figure 4.12. Effect of temperature on kinetic (C_0 = 10 ppm, AD = 4 g/L, and pH = 12)

Kinetic study also continued for geothermal water at the temperatures of 25, 40, 55 °C. Exact procedures were followed as in the lithium model solution. The effects of competitor ions on kinetic of the adsorption were investigated and the results of the study were given in Figure 4.12 and Figure 4.13. For Na^+ and K^+ ions, since maximum of 3% adsorption rate on kinetic at 25 °C and no adsorption rate on kinetics at 40 and 55 °C detected, no figure was presented for these competitor ions. As depicted by the Figure 4.12, lithium adsorption is faster at elevated temperatures, which was the behavior seen in the model lithium solution. However, when model lithium solution investigated, the equilibrium was reached around 8th hour. In the case of geothermal water, even though curves almost plateaus, equilibrium couldn't be reached even in the 24th hour. At the 8th hour, recovery rates were 79, 83, and 88% at 25, 40, and 55 °C and increased to 94% for all tested temperatures at 24th hour. In Figure 4.14, adsorption kinetic of Ca^{2+} and Mg^{2+} were represented in examined temperatures. As well as in lithium adsorption, temperature also accelerated the adsorption rate of competitor ions. Nonetheless, in lithium adsorption, similar adsorption rates were achieved at 24th hours at all temperatures while the equilibrium rates of competitor ions were varied. For Mg^{2+}, when the equilibrium reached at 24th hour, around 6% of adsorption detected at 25 and 40 °C while it was increased to 22% at 55 °C which is notably high. On the other hand, Ca^{2+} did not reach

an equilibrium and kept adsorbing on the adsorbent. Increase in temperature significantly enhanced the Ca^{2+} adsorption from 13% at 25 °C to 22% and 40% at 40 and 55 °C.

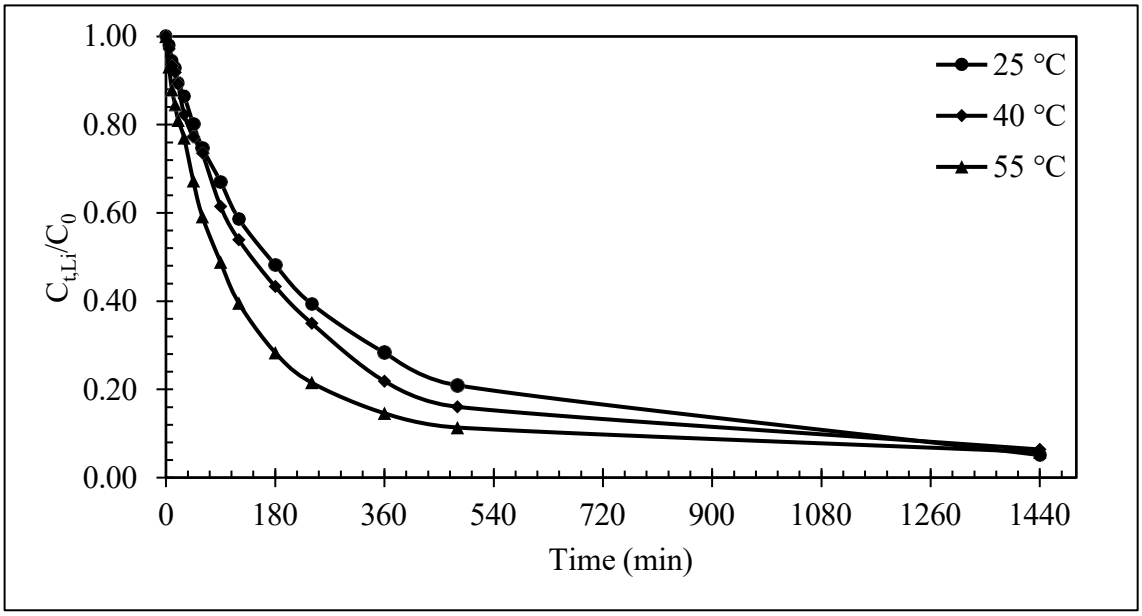

Figure 4.13. Effect of temperature on kinetic of lithium recovery from geothermal water (AD = 4g/L)

Overall, increase in temperature fastens the adsorption kinetics of ion-exchange reaction. It is possible to recover higher concentrations of lithium in shorter times by increasing the temperature. However, considering the increase in the adsorption of competitor ions at elevated temperatures and since lithium recovery unities when the contact time increases, lower temperatures should be considered for an industrial application. Also, the findings from this study proved that the adsorbent selectively excludes the monovalent ions Na^+ and K^+.

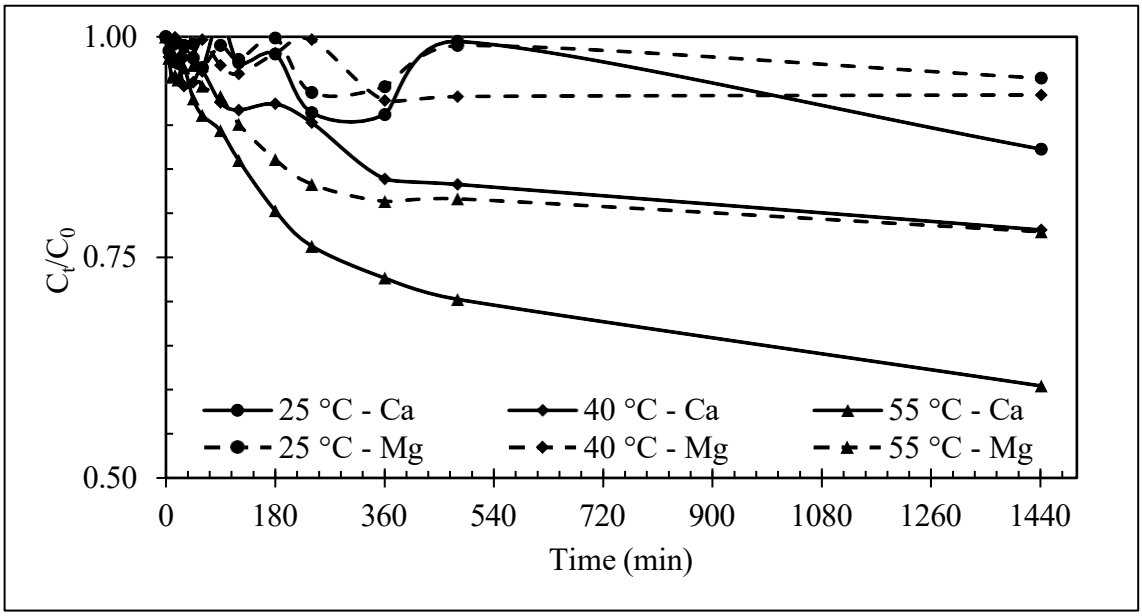

Figure 4.14. Effect of temperature on kinetic behavior of competitor ion recovery from geothermal water (AD = 4g/L, solid line represents the recovery of Ca, while dashed line represents recovery of Mg)

Additionally, another kinetic study was investigated which covers geothermal water with the pH of 12 at 25 °C. It is desired to reveal whether increase in pH of the geothermal water influenced contact time or selectivity to lithium. Figure 4.15 describes the adsorption profile of the Li^+, Mg^{2+}, and Ca^{2+} ions. Change in pH did not have an effect on the adsorption of K^+ and Na^+. Consequently, selective exclusion for these ions persisted, hence they were omitted from the Figure 4.15. In Section 3.4.2, it was proven that the higher alkaline pH of geothermal water resulted in higher lithium recovery rate. At the 8th hour, lithium in the solution was recovered by 97% and reached complete recovery at 24th hour. Also, adsorption rate of lithium was dramatically accelerated, and faster rate compared to geothermal water at 55 °C was achieved and represented in. Nevertheless, the increase in pH did result in increased adsorption rate of divalent competitor ions. At the contact time of 8th hour, 81% Mg^{2+} and 76% Ca^{2+} adsorption was calculated. Thus, increasing the pH of the geothermal water should not be considered as it will result in complexity in purification processes even though it accelerates the ion-exchange reaction and increases the lithium recovery rate.

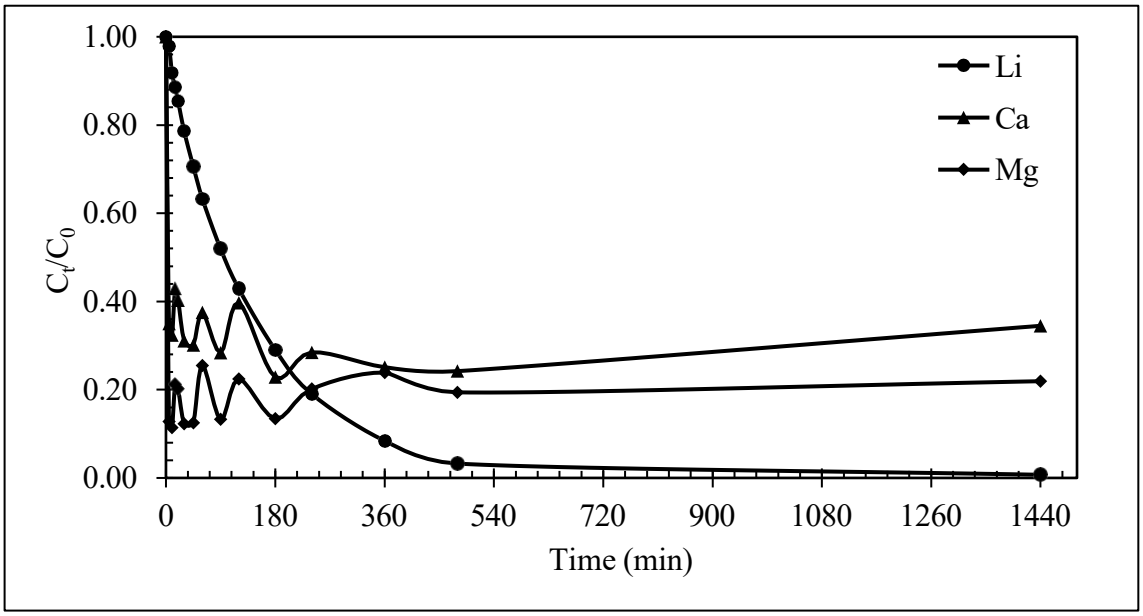

Figure 4.15. Effect of pH on kinetic on geothermal water (pH=12, T = 25 °C, AD = 4 g/L)

Moreover, to understand the kinetic rate, pseudo first order and pseudo second order kinetic rate constants and equilibrium adsorption capacity were calculated as presented in the Table 4.3. It is observed both first and second order regression fit ($R^2 > 0.99$) perfectly and pseudo-second order slight fits better. The relative error between the theoretical adsorption capacity and experimental adsorption capacity were determined to be 7.6% at maximum error while the deviation is lower for the pseudo second order kinetic model. Both first order and second order rate constants were in increasing order with respect to elevation in temperature. An increment of 15 °C from 25 °C resulted in a 35.9% and 20% increase in the reaction rate for pseudo first order and second-order reactions, respectively. A further increment of 15 °C to 55 °C resulted in a 105% and 193% increase for pseudo first order and second-order reactions, respectively, which is significant. This behavior was proven in Section 4.2.8 as the reaction being endothermic. Also, this finding is compatible with the of Figure 4.12.

Table 4.3. Kinetic model parameters of PVC/PAN-HTO on model lithium solution (C_0 = 10 ppm, AD = 4 g/L, pH = 12, V = 750 mL, and RPM = 180)

T (°C)	Pseudo First Order				Pseudo Second Order			
	$q_{e,theo}$ (mg/g)	Error (%)	k_1 (1/min)	R^2	$q_{e,theo}$ (mg/g)	Error (%)	k_2 (g/min/mg)	R^2
25	2.48	7.6	0.0064	0.9971	2.87	7.2	0.0040	0.9984
40	2.53	3.5	0.0087	0.9995	2.81	6.9	0.0048	0.9973
55	2.50	7.0	0.0179	0.9983	2.75	2.6	0.0141	0.9993

Kinetic calculations were also applied for the geothermal water and results of the kinetic study were given in Table 4.4 while no kinetic rate were determined for Na^+ and K^+ as these ions were rejected by adsorbent as aforementioned. Rate constants for Li^+ were found to be increasing order with respect to temperature due to being endothermic reaction as mentioned in Section 4.2.8. The pseudo second order model was deemed to be better fit than pseudo first order model according to the value of R-square. Compared to the study with model lithium solution, the theoretical adsorption capacity ($q_{e,theo}$) is lower when geothermal water was used, as expected since the competitor ions exist while the reaction occurs. Since the R-square values were high ($R^2 > 0.99$), the low relative error between the theoretical adsorption capacity and experimental adsorption capacity was found as 14.9% at maximum and 4.5% at minimum for lithium. An increment of 15 °C from 25 °C resulted in a 26.3% and 33.3% increase in the reaction rate for pseudo first order and second order reactions, respectively. A further increment of 15 °C to 55 °C resulted in a 27% and 114% increase for pseudo-first order and second-order reactions, respectively. Compared to the rate constants obtained from the lithium model solution, effect of temperature on rate is lower when geothermal water was used, yet still considerably high as also presented in Figure 4.12.

Competitor ions, Ca^{2+} and Mg^{2+}, were also considered for the kinetic calculations however the least-square regression method did not result high R-square values for these ions as they were adsorbed and desorbed through the reaction process. For Ca^{2+}, study showed that pseudo-second order model was better fit due to higher R-square values. However, rate constant, k_2, was in decreasing order, inversely with temperature, while the adsorption rate shown to be increased experimentally as given in Figure 4.13. For Mg^{2+}, pseudo first order model was strongly better fit and at 25 °C rate constant yielded

as negative number which can be interpret as little to no Mg^{2+} adsorption while the increase in temperature allowed Mg^{2+} to adsorb on the adsorbent, as the nature of the endothermic adsorption mechanism that will be mentioned in Section 4.2.8 and this behavior experimentally consistent with the finding in Figure 4.13.

Table 4.4. Kinetic model parameters of granulated PVC/PAN-HTO on geothermal water (AD = 4 g/L, V = 750 mL, and RPM = 180)

Ion	T (°C)	Pseudo First Order				Pseudo Second Order			
		$q_{e,theo}$ (mg/g)	Error (%)	k_1 (1/min)	R^2	$q_{e,theo}$ (mg/g)	Error (%)	k_2 (g/min/mg)	R^2
Li	25	1.93	5.1	0.0038	0.9936	2.34	14.9	0.0021	0.9976
	40	1.89	4.5	0.0048	0.9971	2.23	12.6	0.0028	0.9971
	55	1.72	13.6	0.0061	0.9809	2.12	6.2	0.0060	0.9990
Ca	25	0.87	9.0	0.0019	0.3253	0.78	1.6	0.0136	0.4915
	40	1.28	7.8	0.0029	0.9415	1.52	9.3	0.0035	0.9353
	55	1.63	6.5	0.0030	0.9818	1.97	12.6	0.0024	0.9637
Mg	25	0.02	28.3	-0.0054	0.2964	0.03	5.1	-0.6053	0.4751
	40	0.03	17.7	0.0011	0.0736	0.06	44.8	0.0350	0.3169
	55	0.12	4.7	0.0044	0.9396	0.15	17.9	0.0295	0.8827

4.2.7. Adsorption Isotherms

Adsorption isotherms were used to reveal the adsorption behavior of the adsorbent at different temperatures (25, 40, and 55 °C). Langmuir and Freundlich isotherms, which are the most used types, were applied on the data obtained from Section 4.2.3. Langmuir model assumes the single-layer and homogeneous adsorption while Freundlich model includes multilayer adsorption on heterogenous adsorption on surface. Parameters that were calculated by Langmuir and Freundlich isotherms were given in the Table 4.5.

Calculation showed that Langmuir isotherms better describes the experimental data than Freundlich isotherm as the correlation coefficient (R^2) values were higher in Langmuir with the value of 0.99. These results suggest the monolayer homogeneous adsorption of lithium ions on the PVC/PAN-HTO. Based on Langmuir model, the maximum adsorption capacity (q_{max}) were calculated as 5.79 mg/g at 25 °C and decreased to 5.55 and 5.52 mg/g at 40 and 55 °C, respectively. Increase in temperature

led to decrease in the value of K_L, indicating the reduced affinity of binding of lithium ions to adsorbent.

Table 4.5. Isotherm model parameters of PVC/PAN-HTO on different temperatures

Temp. (°C)	Langmuir Adsorption Isotherm Model			Freundlich Adsorption Isotherm Model		
	q_{max} (mg/g)	K_L (L/mg)	R^2	K_F	n	R^2
25	5.88	0.24	0.98	1.96	3.97	0.93
40	5.56	0.32	0.99	2.40	5.22	0.93
55	5.96	0.30	0.99	2.70	5.81	0.87

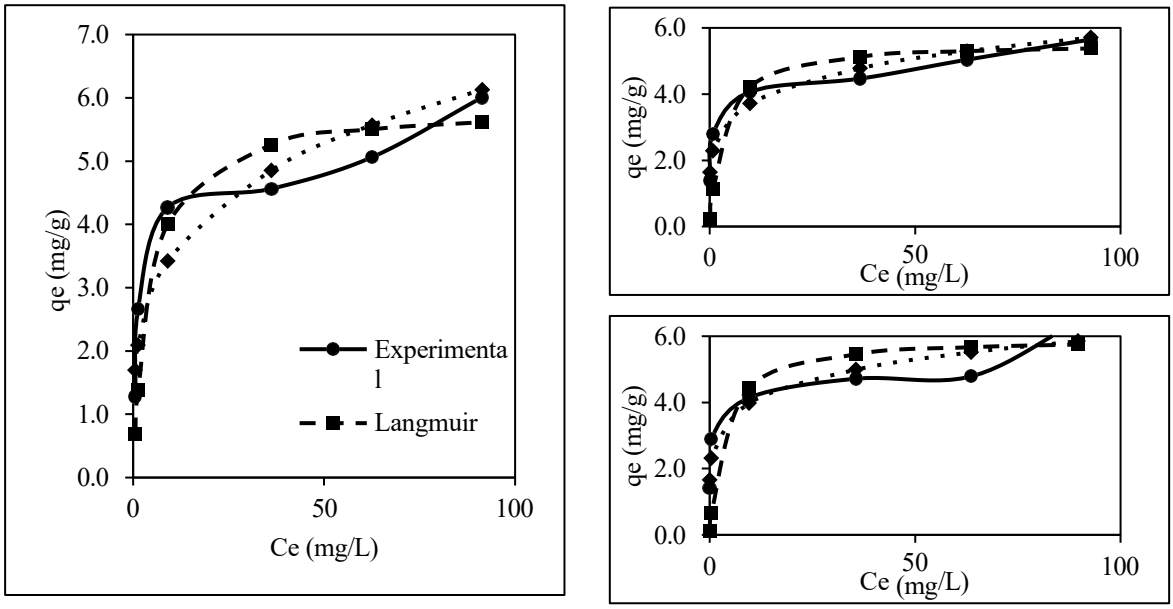

Figure 4.16. Langmuir and Freundlich adsorption isotherms of PVC/PAN-HTO at 25 °C (left), 40 °C (upper right corner), and 55 °C (bottom right corner)

Even though the Langmuir isotherms fits better, Freundlich isotherm also resulted high correlation factors (R^2) (0.93 at 25 and 40 °C, and 0.87 at 55 °C). This finding proves that there might be deviation in adsorption behavior resulting in some level multilayer and/or heterogenous adsorption, especially at lower temperatures. The Freundlich isotherm constant, n, suggest that the adsorption is favorable, non-linear, and

heterogeneous as the value resulted higher than 1 in each temperature.[68] Langmuir and Freundlich isotherms were depicted in Figure 4.16.

4.2.8. Adsorption Thermodynamics

Temperature effect on suggested adsorbent (PVC/PAN-HTO) was also investigated by thermodynamic calculations. In Table 4.6, resulting values of the thermodynamic calculations were given for experimented temperatures of 25, 40, and 55 °C. Increase in temperature decreases the $\Delta G°$ value which indicates higher operating temperature makes the process more spontaneous, thus more favorable.

Table 4.6. Thermodynamics of lithium adsorption on PVC/PAN-HTO

Temperature (°C)	$\Delta G°$ (kJ/mol)	ΔH° (kJ/mol)	ΔS° (kJ/mol.K)
25	-18.49		
40	-19.76	6.73	0.08
55	-21.02		

In general, change in Gibbs free energy of 0 to -20 kJ/mol is correlated with physisorption while the range -80 to -400 kJ/mol is correlated with chemical adsorption.[69] Therefore, adsorption of lithium on the PVC/PAN-HTO is classified as physical adsorption which means lithium is adsorbed with weak physical electrostatic and Van der Waals interactions. By the use of linear analogy of Van't Hoff equation, $\Delta S°$ and $\Delta H°$ were determined from intersection point and slope of the plotted of ln K_e versus $1/T$. Nature of the adsorption process were found to be endothermic, and adsorption decreases with the decreasing temperature, since the $\Delta H°$ value determined as positive. Lastly, change in entropy, $\Delta S°$, calculated as a positive value which indicates that randomness at the solid-liquid interface increases while adsorption process takes place.

CHAPTER 5

CONCLUSION

Global lithium consumption is on an upward trend and expected to be depleted eventually. Considering that lithium extraction is mostly done from lithium mineral ores and since the majority of the lithium is dissolved in the brines, lithium recovery from brines gained attention. Significant improvements made in the literature for a suitable adsorbent however these materials are required to be immobilized to be able to efficiently use in industrial operations.

In this study, immobilized with PVC/PAN granulated titanium-based lithium ion-sieve was synthesized and tested for lithium recovery from water sources. Characterization results (FT-IR, XRD, SEM, and BET) presented that the synthesis of the PVC/PAN-HTO was successful. Adsorbent was tested with varying pH, and it was observed that lithium adsorption reaction should be carried out in alkaline media. For the suggested material, above the point of zero charge value of 6.03 lithium adsorption process takes place while the lower the pH favors the lithium stripping from the adsorbent. Mass of required adsorbent per liter of lithium containing solution experiment was tested on model lithium solution and geothermal water and both resulted the optimum dosage of 4 g/L. Initial lithium concentration experiment resulted that the maximum adsorption capacity of the material was 6.45 mg/g. Adsorption kinetics on model lithium solution and geothermal water were observed and depicted that the reaction rate increased with respect to increase in the temperature while the equilibrium adsorption capacity was remained in united for each temperature tested. Furthermore, study concluded that the synthesized material was highly selective to the lithium, with nearly complete rejection of competing monovalent ions (Na^+ and K^+). Since increase in pH resulted in higher adsorption recovery rates, geothermal water pH was also adjusted for investigation. However, increase in pH resulted in higher selectivity towards Mg^{+2} and deemed as not a feasible alternative. Adsorption isotherms was examined and found that the Langmuir model is better fits than the Freundlich model. The maximum adsorption capacity according to the Langmuir model was calculated as 5.59 mg/g. Thermodynamic studies pointed out that the lithium adsorption process was endothermic as the standard change

in enthalpy was 6.73 kJ/mol. Reaction was categorized as spontaneous and found that the lithium adsorption is physisorption, since the change in Gibbs free energy negative and high, respectively. Desorption study showed that the material exhibits high desorption rate and interprets that the concentration and type of the acid is crucial parameter for stability of it. Furthermore, three adsorption desorption cycles were performed on the adsorbent, and resulted in a 2.07% relative decrease from the initial 96.8% lithium recovery rate. Future research should explore the material under continuous column operation as it is aimed for industrial applications. Additionally, longer-term cycling performance can be investigated.

Research highlights the potential of the titanium-based lithium ion-sieve granulized with PVC and PAN. The findings pave the way for further advancements in this field, ultimately contributing to the development of sustainable and green technology for lithium recovery from water sources.

REFERENCES

1. U.S. Geological Survey. *Mineral Commodity Summaries 2014*; U.S. Geological Survey: Reston, VA, 2014. https://pubs.usgs.gov/publication/70100414 (accessed 2024-05-05).

2. U.S. Geological Survey. *Mineral Commodity Summaries 2024*; U.S. Geological Survey: Reston, VA, 2024. https://pubs.usgs.gov/publication/mcs2024 (accessed 2024-05-05).

3. Orooji, Y.; Nezafat, Z.; Nasrollahzadeh, M.; Shafiei, N.; Afsari, M.; Pakzad, K.; Razmjou, A. Recent Advances in Nanomaterial Development for Lithium Ion-Sieving Technologies. *Desalination* **2022**, *529*. DOI: 10.1016/j.desal.2022.115624.

4. Lin, H.; Yu, X.; Li, M.; Duo, J.; Guo, Y.; Deng, T. Synthesis of Polyporous Ion-Sieve and Its Application for Selective Recovery of Lithium from Geothermal Water. *ACS Appl. Mater. Interfaces* **2019**, *11* (29), 26364–26372. DOI: 10.1021/acsami.9b07401.

5. Swain, B. Recovery and Recycling of Lithium: A Review. *Sep. Purif. Technol.* **2017**, *172*, 388–403. DOI: 10.1016/j.seppur.2016.08.031.

6. Xu, X.; Chen, Y.; Wan, P.; Gasem, K.; Wang, K.; He, T.; Adidharma, H.; Fan, M. Extraction of Lithium with Functionalized Lithium Ion-Sieves. *Prog. Mater. Sci.* **2016**, *84*, 276–313. DOI: 10.1016/j.pmatsci.2016.09.004.

7. Ryu, T.; Haldorai, Y.; Rengaraj, A.; Shin, J.; Hong, H. J.; Lee, G. W.; Han, Y. K.; Huh, Y. S.; Chung, K. S. Recovery of Lithium Ions from Seawater Using a Continuous Flow Adsorption Column Packed with Granulated Chitosan-Lithium Manganese Oxide. *Ind. Eng. Chem. Res.* **2016**, *55* (26), 7218–7225. DOI: 10.1021/acs.iecr.6b01632.

8. Udoetok, I. A.; Karoyo, A. H.; Ubuo, E. E.; Asuquo, D. E. Granulation of Lithium-Ion Sieves (LISs) Using Biopolymers: A Review. *Preprints (Basel)* **2024**. DOI: 10.20944/preprints202402.0329.v1.

9. Kavanagh, L.; Keohane, J.; Cabellos, G. G.; Lloyd, A.; Cleary, J. Global Lithium Sources-Industrial Use and Future in the Electric Vehicle Industry: A Review. *Resources* **2018**, *7* (3). DOI: 10.3390/resources7030057.

10. Chandrasekharam, D.; Şener, M. F.; Recepoğlu, Y. K.; Isık, T.; Demir, M. M.; Baba, A. Lithium: An Energy Transition Element, Its Role in the Future Energy Demand and Carbon Emissions Mitigation Strategy. *Geothermics* **2024**, *119*. DOI: 10.1016/j.geothermics.2024.102959.

11. Heredia, F.; Martinez, A. L.; Surraco Urtubey, V. The Importance of Lithium for Achieving a Low-Carbon Future: Overview of the Lithium Extraction in the 'Lithium Triangle.' *J. Energy Nat. Resources L.* **2020**, *38* (3), 213–236. DOI: 10.1080/02646811.2020.1784565.

12. Miatto, A.; Wolfram, P.; Reck, B. K.; Graedel, T. E. Uncertain Future of American Lithium: A Perspective until 2050. *Environ. Sci. Technol.* **2021**, *55* (23), 16184–16194. DOI: 10.1021/acs.est.1c03562.

13. Kim, S.; Joo, H.; Moon, T.; Kim, S. H.; Yoon, J. Rapid and Selective Lithium Recovery from Desalination Brine Using an Electrochemical System. *Environ. Sci. Process Impacts* **2019**, *21* (4), 667–676. DOI: 10.1039/c8em00498f.

14. Weng, D.; Duan, H.; Hou, Y.; Huo, J.; Chen, L.; Zhang, F.; Wang, J. Introduction of Manganese Based Lithium-Ion Sieve-A Review. *Prog. Nat. Sci.: Mater. Int.* **2020**, *30* (2), 139–152. DOI: 10.1016/j.pnsc.2020.01.017.

15. Silvana, V. K.; Horacio, F. R.; Agustina, O. M. Influence of The Evaporation Rate Over Lithium Recovery From Brines. *World J. Res. Rev.* **2016**, No. 1, 66.

16. Meshram, P.; Pandey, B. D.; Mankhand, T. R. Extraction of Lithium from Primary and Secondary Sources by Pre-Treatment, Leaching and Separation: A Comprehensive Review. *Hydrometallurgy* **2014**, *150*, 192–208. DOI: 10.1016/j.hydromet.2014.10.012.

17. Alsabbagh, A.; Aljarrah, S.; Almahasneh, M. Lithium Enrichment Optimization from Dead Sea End Brine by Chemical Precipitation Technique. *Miner. Eng.* **2021**, *170*. DOI: 10.1016/j.mineng.2021.107038.

18. Kanagasundaram, T.; Murphy, O.; Haji, M. N.; Wilson, J. J. The Recovery and Separation of Lithium by Using Solvent Extraction Methods. *Coord. Chem. Rev.* **2024**, *509*. DOI: 10.1016/j.ccr.2024.215727.

19. Zhou, Z.; Fan, J.; Liu, X.; Hu, Y.; Wei, X.; Hu, Y.; Wang, W.; Ren, Z. Recovery of Lithium from Salt-Lake Brines Using Solvent Extraction with TBP as Extractant and FeCl3 as Co-Extraction Agent. *Hydrometallurgy* **2020**, *191*. DOI: 10.1016/j.hydromet.2019.105244.

20. Stringfellow, W. T.; Dobson, P. F. Technology for the Recovery of Lithium from Geothermal Brines. *Energies (Basel)* **2021**, *14* (20). DOI: 10.3390/en14206805.

21. Nie, X. Y.; Sun, S. Y.; Sun, Z.; Song, X.; Yu, J. G. Ion-Fractionation of Lithium Ions from Magnesium Ions by Electrodialysis Using Monovalent Selective Ion-Exchange Membranes. *Desalination* **2017**, *403*, 128–135. DOI: 10.1016/j.desal.2016.05.010.

22. Chen, S.; Chen, Z.; Wei, Z.; Hu, J.; Guo, Y.; Deng, T. Titanium-Based Ion Sieve with Enhanced Post-Separation Ability for High Performance Lithium Recovery from Geothermal Water. *Chem. Eng. J.* **2021**, *410*. DOI: 10.1016/j.cej.2020.128320.

23. Chitrakar, R.; Makita, Y.; Ooi, K.; Sonoda, A. Lithium Recovery from Salt Lake Brine by H_2TiO_3. *Dalton Trans.* **2014**, *43* (23), 8933–8939. DOI: 10.1039/c4dt00467a.

24. Xu, W.; He, L.; Zhao, Z. Lithium Extraction from High Mg/Li Brine via Electrochemical Intercalation/de-Intercalation System Using $LiMn_2O_4$ Materials. *Desalination* **2021**, *503*. DOI: 10.1016/j.desal.2021.114935.

25. Li, X.; Chao, Y.; Chen, L.; Chen, W.; Luo, J.; Wang, C.; Wu, P.; Li, H.; Zhu, W. Taming Wettability of Lithium Ion Sieve via Different TiO_2 Precursors for Effective Li Recovery from Aqueous Lithium Resources. *Chem. Eng. J.* **2020**, *392*. DOI: 10.1016/j.cej.2019.123731.

26. Moazeni, M.; Hajipour, H.; Askari, M.; Nusheh, M. Hydrothermal Synthesis and Characterization of Titanium Dioxide Nanotubes as Novel Lithium Adsorbents. *Mater. Res. Bull.* **2015**, *61*, 70–75. DOI: 10.1016/j.materresbull.2014.09.069.

27. Xiao, J.; Nie, X.; Sun, S.; Song, X.; Li, P.; Yu, J. Lithium Ion Adsorption-Desorption Properties on Spinel $Li_4Mn_5O_{12}$ and PH-Dependent Ion-Exchange Model. *Adv. Powder Technol.* **2015**, *26* (2), 589–594. DOI: 10.1016/j.apt.2015.01.008.

28. Xiao, J. L.; Sun, S. Y.; Wang, J.; Li, P.; Yu, J. G. Synthesis and Adsorption Properties of $Li_{1.6}Mn_{1.6}O_4$ Spinel. *Ind. Eng. Chem. Res.* **2013**, *52* (34), 11967–11973. DOI: 10.1021/ie400691d.

29. Zhang, Q. H.; Sun, S.; Li, S.; Jiang, H.; Yu, J. G. Adsorption of Lithium Ions on Novel Nanocrystal MnO_2. *Chem. Eng. Sci.* **2007**, *62* (18–20), 4869–4874. DOI: 10.1016/j.ces.2007.01.016.

30. Nisola, G. M.; Limjuco, L. A.; Vivas, E. L.; Lawagon, C. P.; Park, M. J.; Shon, H. K.; Mittal, N.; Nah, I. W.; Kim, H.; Chung, W. J. Macroporous Flexible Polyvinyl Alcohol Lithium Adsorbent Foam Composite Prepared via Surfactant Blending and Cryo-Desiccation. *Chem. Eng. J.* **2015**, *280*, 536–548. DOI: 10.1016/j.cej.2015.05.107.

31. Ma, L. W.; Chen, B. Z.; Chen, Y.; Shi, X. C. Preparation, Characterization and Adsorptive Properties of Foam-Type Lithium Adsorbent. *Microporous and Mesoporous Mater.* **2011**, *142* (1), 147–153. DOI: 10.1016/j.micromeso.2010.11.028.

32. Limjuco, L. A.; Nisola, G. M.; Lawagon, C. P.; Lee, S. P.; Seo, J. G.; Kim, H.; Chung, W. J. H_2TiO_3 Composite Adsorbent Foam for Efficient and Continuous Recovery of Li^+ from Liquid Resources. *Colloids. Surf. A Physicochem. Eng. Asp.* **2016**, *504*, 267–279. DOI: 10.1016/j.colsurfa.2016.05.072.

33. Xu, P.; Hong, J.; Qian, X.; Xu, Z.; Xia, H.; Tao, X.; Xu, Z.; Ni, Q. Q. Materials for Lithium Recovery from Salt Lake Brine. *J. Mater. Sci.* **2021**, *56* (1), 16–63. DOI: 10.1007/s10853-020-05019-1.

34. Park, M. J.; Nisola, G. M.; Beltran, A. B.; Torrejos, R. E. C.; Seo, J. G.; Lee, S. P.; Kim, H.; Chung, W. J. Recyclable Composite Nanofiber Adsorbent for Li^+ Recovery from Seawater Desalination Retentate. *Chem. Eng. J.* **2014**, *254*, 73–81. DOI: 10.1016/j.cej.2014.05.095.

35. Zhao, K.; Tong, B.; Yu, X.; Guo, Y.; Xie, Y.; Deng, T. Synthesis of Porous Fiber-Supported Lithium Ion-Sieve Adsorbent for Lithium Recovery from Geothermal Water. *Chem. Eng. J.* **2022**, *430*. DOI: 10.1016/j.cej.2021.131423.

36. Lawagon, C. P.; Nisola, G. M.; Cuevas, R. A. I.; Kim, H.; Lee, S. P.; Chung, W. J. Development of High Capacity Li^+ Adsorbents from H_2TiO_3/Polymer Nanofiber Composites: Systematic Polymer Screening, Characterization and Evaluation. *J. Ind. Eng. Chem.* **2019**, *70*, 124–135. DOI: 10.1016/j.jiec.2018.10.003.

37. Umeno, A.; Miyai, Y.; Takagi, N.; Chitrakar, R.; Sakane, K.; Ooi, K. Preparation and Adsorptive Properties of Membrane-Type Adsorbents for Lithium Recovery from Seawater. *Ind. Eng. Chem. Res.* **2002**, *41* (17), 4281–4287. DOI: 10.1021/ie010847j.

38. Zhu, G.; Wang, P.; Qi, P.; Gao, C. Adsorption and Desorption Properties of Li+ on PVC-$H_{1.6}Mn_{1.6}O_4$ Lithium Ion-Sieve Membrane. *Chem. Eng. J.* **2014**, *235*, 340–348. DOI: 10.1016/j.cej.2013.09.068.

39. Sun, D.; Meng, M.; Yin, Y.; Zhu, Y.; Li, H.; Yan, Y. Highly Selective, Regenerated Ion-Sieve Microfiltration Porous Membrane for Targeted Separation of Li^+. *J. Porous Mater.* **2016**, *23* (6), 1411–1419. DOI: 10.1007/s10934-016-0201-4.

40. Min, K.; Cuiffi, J. D.; Mathers, R. T. Ranking Environmental Degradation Trends of Plastic Marine Debris Based on Physical Properties and Molecular Structure. *Nat. Commun.* **2020**, *11* (1). DOI: 10.1038/s41467-020-14538-z.

41. Wang, H.; Cui, J.; Li, M.; Guo, Y.; Deng, T.; Yu, X. Selective Recovery of Lithium from Geothermal Water by EGDE Cross-Linked Spherical CTS/LMO. *Chem. Eng. J.* **2020**, *389*. DOI: 10.1016/j.cej.2020.124410.

42. Qian, H.; Huang, S.; Ba, Z.; Wang, W.; Yu, F.; Liang, D.; Xie, Y.; Wang, Y.; Wang, Y. HTO/Cellulose Aerogel for Rapid and Highly Selective Li+ Recovery from Seawater. *Molecules* **2021**, *26* (13). DOI: 10.3390/molecules26134054.

43. Xiao, G.; Tong, K.; Zhou, L.; Xiao, J.; Sun, S.; Li, P.; Yu, J. Adsorption and Desorption Behavior of Lithium Ion in Spherical PVC-MnO_2 Ion Sieve. *Ind. Eng. Chem. Res.* **2012**, *51* (33), 10921–10929. DOI: 10.1021/ie300087s.

44. Xiao, J. L.; Sun, S. Y.; Song, X.; Li, P.; Yu, J. G. Lithium Ion Recovery from Brine Using Granulated Polyacrylamide-MnO_2 Ion-Sieve. *Chem. Eng. J.* **2015**, *279*, 659–666. DOI: 10.1016/j.cej.2015.05.075.

45. Zhang, C.; Yao, J.; Zhai, W.; Chen, H.; He, H.; Zhang, Y. B.; He, T. Lithium Extraction from Geothermal Brine by Granulated HTO Titanium-Based Adsorbent with Block-Co-Polymer Poly (Ethylene-Co-Vinyl Alcohol) (EVAL) as Binder. *Chem. Eng. J.* **2023**, *467*. DOI: 10.1016/j.cej.2023.143526.

46. Zhang, G.; Hai, C.; Zhou, Y.; Zhang, J.; Liu, Y.; Zeng, J.; Shen, Y.; Li, X.; Sun, Y.; Wu, Z.; Tang, W. Synthesis and Performance Estimation of a Granulated PVC/PAN-Lithium Ion-Sieve for Li+ Recovery from Brine. *Sep. Purif. Technol.* **2023**, *305*. DOI: 10.1016/j.seppur.2022.122431.

47. Li, H.; Qin, J.; Zhao, K.; Guo, Y.; Tong, B.; Samadiy, M.; Alimov, U.; Deng, T. Novel Lithium Ion-Sieve Spinning Fiber Composite of PVDF-HMO for Lithium Recovery from Geothermal Water. *J. Clean. Prod.* **2024**, *434*. DOI: 10.1016/j.jclepro.2023.139997.

48. Zhang, L.; Zhou, D.; He, G.; Yao, Q.; Wang, F.; Zhou, J. Synthesis of H2TiO3-Lithium Adsorbent Loaded on Ceramic Foams. *Mater. Lett.* **2015**, *145*, 351–354. DOI: 10.1016/j.matlet.2015.01.142.

49. Hong, H. J.; Ryu, T.; Park, I. S.; Kim, M.; Shin, J.; Kim, B. G.; Chung, K. S. Highly Porous and Surface-Expanded Spinel Hydrogen Manganese Oxide (HMO)/Al_2O_3 Composite for Effective Lithium (Li) Recovery from Seawater. *Chem. Eng. J.* **2018**, *337*, 455–461. DOI: 10.1016/j.cej.2017.12.130.

50. Hong, H. J.; Park, I. S.; Ryu, J.; Ryu, T.; Kim, B. G.; Chung, K. S. Immobilization of Hydrogen Manganese Oxide (HMO) on Alpha-Alumina Bead (AAB) to Effective Recovery of Li+ from Seawater. *Chem. Eng. J.* **2015**, *271*, 71–78. DOI: 10.1016/j.cej.2015.02.023.

51. Koilraj, P.; Smith, S. M.; Yu, Q.; Ulrich, S.; Sasaki, K. Encapsulation of a Powdery Spinel-Type Li+ Ion Sieve Derived from Biogenic Manganese Oxide in Alginate Beads. *Powder Technol.* **2016**, *301*, 1201–1207. DOI: 10.1016/j.powtec.2016.08.009.

52. Hong, H. J.; Park, I. S.; Ryu, T.; Kim, B. G.; Chung, K. S. Macroporous Hydrogen Manganese Oxide/Al_2O_3 for Effective Lithium Recovery from Seawater: Effects of the Macropores vs Mesopores. *Ind. Eng. Chem. Res.* **2019**, *58* (19), 8342–8348. DOI: 10.1021/acs.iecr.9b01613.

53. Zandvakili, S.; Ranjbar, M. Preparation and Characterisation of Lithium Ion Exchange Composite for the Recovery of Lithium from Brine. *Miner. Process. Extr. Metall.: Trans. Inst. Min. Metall.* **2018**, *127* (3), 176–181. DOI: 10.1080/03719553.2017.1334983.

54. Ding, W.; Zhang, J.; Liu, Y.; Guo, Y.; Deng, T.; Yu, X. Synthesis of Granulated $H_4Mn_5O_{12}$/Chitosan with Improved Stability by a Novel Cross-Linking Strategy for Lithium Adsorption from Aqueous Solutions. *Chem. Eng. J.* **2021**, *426*. DOI: 10.1016/j.cej.2021.131689.

55. Zhang, Y.; Liu, J.; Yang, Y.; Lin, S.; Li, P. Preparation of Granular Titanium-Type Lithium-Ion Sieves and Recyclability Assessment for Lithium Recovery from Brines with Different PH Value. *Sep. Purif. Technol.* **2021**, *267*. DOI: 10.1016/j.seppur.2021.118613.

56. Hong, H. J.; Park, I. S.; Ryu, T.; Ryu, J.; Kim, B. G.; Chung, K. S. Granulation of $Li_{1.33}Mn_{1.67}O_4$ (LMO) through the Use of Cross-Linked Chitosan for the Effective Recovery of Li+ from Seawater. *Chem. Eng. J.* **2013**, *234*, 16–22. DOI: 10.1016/j.cej.2013.08.060.

57. Yang, Z.; Li, Y.; Ma, P. Synthesis of H2TiO3-PVC Lithium-Ion Sieves via an Antisolvent Method and Its Adsorption Performance. *Ceram. Int.* **2022**, *48* (20), 30127–30134. DOI: 10.1016/j.ceramint.2022.06.284.

58. Lai, X.; Yuan, Y.; Chen, Z.; Peng, J.; Sun, H.; Zhong, H. Adsorption-Desorption Properties of Granular EP/HMO Composite and Its Application in Lithium Recovery from Brine. *Ind. Eng. Chem. Res.* **2020**, *59* (16), 7913–7925. DOI: 10.1021/acs.iecr.0c00668.

59. Qiu, Z.; Wang, M.; Chen, Y.; Zhang, T.; Yang, D.; Qiu, F. Li4Mn5O12 Doped Cellulose Acetate Membrane with Low Mn Loss and High Stability for Enhancing Lithium Extraction from Seawater. *Desalination* **2021**, *506*. DOI: 10.1016/j.desal.2021.115003.

60. Jia, Q.; Wang, J.; Guo, R. Preparation and Characterization of Porous HMO/PAN Composite Adsorbent and Its Adsorption–Desorption Properties in Brine. *J. Porous Mater.* **2019**, *26* (3), 705–716. DOI: 10.1007/s10934-018-0662-8.

61. Han, Y.; Kim, H.; Park, J. Millimeter-Sized Spherical Ion-Sieve Foams with Hierarchical Pore Structure for Recovery of Lithium from Seawater. *Chem. Eng. J.* **2012**, *210*, 482–489. DOI: 10.1016/j.cej.2012.09.019.

62. Simonin, J. P. On the Comparison of Pseudo-First Order and Pseudo-Second Order Rate Laws in the Modeling of Adsorption Kinetics. *Chem. Eng. J.* **2016**, *300*, 254–263. DOI: 10.1016/j.cej.2016.04.079.

63. Langmuir, I. The Constitution and Fundamental Properties of Solids and Liquids. *J. Am. Chem. Soc.* **1916**, *38* (11), 2221–2295. DOI: https://doi.org/10.1021/ja02268a002.

64. Freundlich, H. Über Die Adsorption in Lösungen. *J. Phys. Chem.* **1907**, *57U* (1), 385–470. DOI: https://doi.org/10.1515/zpch-1907-5723.

65. Lima, E. C.; Gomes, A. A.; Tran, H. N. Comparison of the Nonlinear and Linear Forms of the van't Hoff Equation for Calculation of Adsorption Thermodynamic Parameters (ΔS° and ΔH°). *J. Mol. Liq.* **2020**, *311*. DOI: 10.1016/j.molliq.2020.113315.

66. Recepoğlu, Y. K.; Arabacı, B.; Kahvecioğlu, A.; Yüksel, A. Granulation of Hydrometallurgically Synthesized Spinel Lithium Manganese Oxide Using Cross-Linked Chitosan for Lithium Adsorption from Water. *J. Chromatogr. A* **2024**, *1719*. DOI: 10.1016/j.chroma.2024.464712.

67. Helfferich, F.G. *Ion Exchange*; Courier Corporation, 1995.

68. Ruthven, M. R. *Principles of Adsorption and Adsorption Processes*; John Wiley & Sons, 1984.

69. Wang, Y.; Mu, Y.; Zhao, Q. B.; Yu, H. Q. Isotherms, Kinetics and Thermodynamics of Dye Biosorption by Anaerobic Sludge. *Sep. Purif. Technol.* **2006**, *50* (1), 1–7. DOI: 10.1016/j.seppur.2005.10.012.